Structural analysis and shape-preferred orientation determination of the mélange facies in the Chañaral mélange, Las Tórtolas Formation, Coastal Cordillera, northern Chile.

Paulina Fuentes[a], Juan Díaz-Alvarado[a,*], Carlos Fernández[b], Manuel Díaz-Azpiroz[c], Natalia Rodríguez[a]

[a] *Departamento de Geología, Universidad de Atacama, Copayapu 485, Copiapó, Chile*

[b] *Departamento de Geodinámica y Paleontología, Universidad de Huelva, E-21071 Huelva, Spain*

[c] *Departamento de Sistemas Físicos, Químicos y Naturales, Universidad Pablo de Olavide, 41013 Seville, Spain*

ABSTRACT

This study sheds light on the tectonic and structural knowledge of the mélange facies located to the south of Chañaral city, Chile. The Chañaral mélange has been related to an accretionary prism at the western active continental margin of Gondwana. Based on the fossil content, the original turbidite sequence would have been deposited during Devonian to Carboniferous times.

The Chañaral mélange is included in the Las Tórtolas Formation, which corresponds to the Paleozoic metasedimentary basement located in the Coastal Range in northern Chile. It consists of a monotonous sequence of more than 90% of interbedded sandstones and shales, with a few limestones, pelagic chert, conglomerates and basic volcanic rocks, metamorphosed to the greenschist facies. In the study area, the Las Tórtolas Formation is divided into two structural domains separated by a major reverse dextral structure, called here the Infieles fault. To the east, the Las Tórtolas Formation is characterized by a brittle-ductile deformation, defined by the original sedimentary contacts in the turbiditic sequence. Besides, thrust faults and associated thrust propagation folds promotes a penetrative axial plane foliation. Mélange facies are located to the west of the Infieles fault. Although lithologies comprising this domain are similar to the rest of the Las Tórtolas Formation, mélange facies (ductile domain) are characterized by the complete disruption of the original architecture of the turbidite succession. The most significant structures in the mélange are the ubiquitous boudinage and pinch and swell structures, asymmetric objects, S-C structures and tight to isoclinal folds. This deformation is partitioned in the Chañaral mélange between linear fabric domains (L), characterized by quartzite blocks with prolate shape in a phyllite matrix with pencil structures, and linear-planar fabric domains (L-S), where quartzite objects show oblate shape and phyllites present a penetrative foliation. The intensity of deformational process is

reflected in the high aspect ratios yielded by the quartzite constrictive (L) and flattened (L-S) object axes.

Meso-scale shape preferred orientation (SPO) has been compared with quartz microtextures in quartzite blocks, resulting aspect ratios considerably lower than those obtained from the mesoscopic fabric. Main deformation mechanism observed in quartz microtextures are bulging-subgrain rotation recrystallization and dissolution-precipitation creep for pure and impure quartzites respectively. The temperatures deduced from these microtextures are between 350 and 400 ºC, which coincides with the greenschists facies metamorphism observed in the Las Tórtolas and the mélange facies. Extremely dissociation between micro- and meso-scale deformation could be generated by dissolution at high differential stress in the boundaries of the quartzite layers and precipitation at low differential stress parts, which would increase the aspect ratio of the lenses whereas internally, quartz would have remained virtually unstrained.

We propose here a tectonic setting for the Chañaral mélange formation based on the geodynamic evolution of the western active margin of South America during Late Paleozoic to Early Jurassic. Thus, the study area is located in a LT-HP zone of an accretionary complex, where rocks from the subduction channel (mélange facies) and the basal domain of the prism (brittle-ductile domain of the Las Tórtolas Formation) are in contact through the Infieles fault.

Keywords: Mélange, SPO, microfabric, ellipsoid, subduction channel

1.- Introduction

Mélanges and broken formations are defined as mixed rock bodies and exotic blocks yielding different ages, origins and/or dissimilar metamorphic grades (Cloos, 1982; Festa et al., 2010, 2012), which are included in a fine-grained matrix (Raymond, 1984), where the stratigraphic continuity has been completely disrupted at a scale of meters to tens of meters (Festa et al., 2010, 2012; Silver and Beutner, 1980). The significance of mélange has been hotly debated and is often associated with other terms, such as wildflysch, argille scagliose, olistostromes, megabreccias and agglomerates (Camerlenghi and Pini, 2009), depending on the different interpretations of its origin. More recently, the term mélange has been preferably used as a descriptive and non-genetic concept describing mappable rock bodies showing the characteristics mentioned above (Festa et al., 2012). The mélange internal structure may result from different processes, such as tectonic deformations,

68 massive transport, diapirism or hydro-fracturing, that is associated with the interstitial pressure in
69 unconsolidated to not entirely consolidated sediments at shallow crustal levels, facilitating a brittle
70 but mesoscopically continuous deformation (Talbot and von Brunn, 1989; Maltman and Bolton,
71 2003; Festa et al., 2010).
72 Chaotic mélange-like rock formations have been described worldwide, and they play an important
73 role in different geological environments (Festa et al., 2010). Mélanges and olistostromes related to
74 a pre-collisional subduction/obduction and/or accretionary tectonic context have been defined in the
75 Alps (Federico et al., 2007) and in older orogens, such as the Appalachians (Williams and Hatcher,
76 1983). These olistostromes are commonly generated at the front and the base of the accretionary
77 wedge (i. e., the Franciscan Complex: Hsü, 1968; Cowan 1985; Shimanto Belt: Taira et al., 1992;
78 Yamamoto et al., 2007; Kodiak Complex: Vrolijk et al., 1988). In addition, the accretionary
79 complexes may also include mud volcanoes and diapirs (Westbrook and Smith, 1983). Moreover,
80 olistostromes and olistolites have been related to extensional tectonics during rifting or formation in
81 front of the accretionary wedge during the post-collisional stage, as in the Himalayas (Dilek et al.,
82 2010; Festa et al., 2010).
83 The development of accretionary complexes achieves great significance for cortical growth
84 processes, either by the basal or frontal accretion of oceanic material along the prism or the building
85 of voluminous magmatic arcs (i. e., Closs and Shreve, 1988; Condie, 2007; Cawood et al., 2009).
86 According to their origins, Festa et al. (2010, 2012) have identified two mélange subtypes related to
87 subduction in convergent margins. Mass-transport deposits located in the frontal accretionary prism
88 are characterized by chaotic organization and different degrees of stratal disruption. The extra-basin
89 rocks are presented as blocks, olistostromes and olistoliths preserving their subduction-related
90 fabrics in a fine-grained matrix (Festa et al., 2010, 2012; Bortolotti *et al.,* 2004, Abbate *et al.,* 1970;
91 Pini, 1999). Moreover, tectonic broken formations and mélanges show structural and lithological
92 evidence of various degrees of mixing and deformation depending on the rheology of the involved
93 materials, the superposition of different tectonic phases and the discontinuous participation of
94 subduction-related processes as layer-parallel extensions, such as underthrusting, fluidization,
95 forced return flows or block stacking (Lash, 1987; Ujiie, 2002; Cousineau, 1998; Yamamoto et al.,
96 2000, 2009; Pini, 1999; Niwa, 2006, Grigull et al., 2012). Among the most relevant structures
97 present in these formations are pinch-and-swell structures, boudins, isoclinal folds, sheath folds, S-
98 C-C′ structures, slump folds, slump balls, extensional and thrust duplexes, joint systems, hackle
99 fringes and plumose structures (Festa et al., 2010; Taira et al., 1992; Pini, 1999; Yamamoto et al.,
100 2007; Ohsumi and Ogawa, 2008; Vannucchi and Bettelli, 2002; Bettelli and Vannucchi, 2003). The
101 vergences of the structures formed during the process of stratal disruption coincide with the relative

motions of the convergent tectonic plates (i. e., Shi et al., 2013; Escuder-Viruete and Baumgartner, 2014; Kato and Godoy, 2015).

Regarding the mélange facies formed during the underplating of subduction channel materials beneath the overlying accretionary prism, stratal disruption is controlled by the physical properties of sediments at shallow structural levels, whereas during the downward motion of mélange materials, the brittle and ductile shearing structures described above are dominant to acquire mélange fabrics (Ujiie, 2002; Escuder-Viruete and Baumgartner, 2014). The progressive deformation and final mélange textures are determined by the interplay and location of the diffuse transition between unconsolidated and lithified sediments during the progressive increase of the degree of consolidation and metamorphic mineral transformation (Byrne, 1994; Festa et al., 2012; Kato and Godoy, 2015). The scarce microstructural studies carried out in mélange matrix show that dissolution–precipitation creep, and not crystal plastic deformation, controls the deformation distribution (Grigull et al., 2012). Moreover, there is broad agreement that the rheology of the mélange facies is determined by the flowing matrix behavior, with a minor influence of blocks (Cloos, 1982; Shreve and Cloos, 1986; Grigull et al., 2012).

This article attempts to order the sequence of structures that form the architecture of the mélange facies in the Chañaral area in northern Chile, which belongs to a north-south mélange formation alignment on the western margin of South America and is tectonically related to an accretionary complex active between the Late Paleozoic and the Early Andean cycle (Hervé, 1988; Brandon and Calderwood 1990; Mortimer, 1993; Deckert et al., 2002; Kato and Godoy, 2015). The organization and vergence of the structures present in the mélange facies, along with the analysis of the macroscopic and microscopic fabrics in the different structural domains, allow us to determine the processes involved in generating mélange facies textures and their locations within the tectonic context of the accretionary complexes.

2.- Geological setting

The geology of the western margin of South America is determined by its tectonic context as an active continental margin. Its evolution from the Late Proterozoic to Late Paleozoic was marked by the accretion of exotic terranes and migration of the arc to the west (Charrier et al., 2007; Hervé et al., 2007, 2013). The period between the Late Permian and Early Jurassic involves a cessation or deceleration of the subduction process, which coincided with the final configuration of the Pangea supercontinent. Thermal anomalies generated in the lithospheric mantle during this period are

136 conducive to the conditions for partial melting in the lower crust and the emplacement of mainly S-
137 type magmas. Late Paleozoic metasedimentary rocks and Triassic intrusives conform the basement
138 for Jurassic-Cretaceous magmatic arc development during the subsequent fragmentation of
139 Gondwana and the reactivation of subduction (Ramos, 1999; Charrier et a., 2007; Mpodozis and
140 Ramos, 2008). During the NW-SE trending oblique convergence of the Phoenix and Southamerican
141 plates, the high angle of subduction favored the negative velocity of trench roll-back (Mpodozis and
142 Ramos, 2008), and a crustal extensional context was established in the western continental margin
143 of South America (Ramos, 1999; Charrier et al., 2007; Mpodozis and Ramos, 2008). Extensional to
144 transtensive deformational conditions were maintained up to the Late Cretaceous (Mpodozis and
145 Ramos, 2008; Charrier et al., 2007), when a compressive deformational phase occurred in northern
146 Chile, with flexural slip folding and thrusting structures that compose a classic pattern of "thin-
147 skinned" tectonics (i. e., Grocott and Taylor, 2002; Arévalo and Grocott, 1997). This Late Paleozoic
148 to Cenozoic deformational sequence corresponds to a positive tectonic inversion (Williams et al.,
149 1989).
150 The Las Tórtolas Formation, designated as part of the metasedimentary basement of the Coastal
151 Cordillera of northern Chile (Bell, 1982), presents an extremely deformed domain, named mélange
152 facies or Chañaral mélange, characterised by blocks of sandstone in a pelitic matrix (Bell, 1982;
153 Bell, 1987). The structural configuration of the Las Tórtolas Formation has been linked to the
154 tectonic context of an accretionary wedge resulting from the overlapping of several complex
155 deformational events affecting unlithified sediments (Bell, 1987). In central Chile, the accretionary
156 wedge has been divided into two metamorphic series: the intermediate- to high-pressure Western
157 Series and the low-pressure Eastern Series (Aguirre et al., 1972), which comprise, respectively, the
158 deeper and shallower levels of the accretionary complex (Willner et al., 2005).
159
160 *Las Tórtolas Formation*
161 The Las Tórtolas Formation consists of a monotonous sequence of interbedded sandstones and
162 shales, with a few limestones, pelagic chert, conglomerates and basic volcanic rocks. It was
163 tectonically deformed and metamorphosed to the greenschist facies (Miller 1970; Aguirre et al.
164 1972) during the Late Carboniferous to Early Permian. The basement of the Las Tórtolas Formation
165 is unknown, while the Pan de Azúcar and Cifuncho formations are unconformably deposited over it.
166 The Las Tórtolas Formation extends as a NNE-trending continuous 12 km wide strip from Sierra
167 Matancilla to Quebrada Chañaral (Naranjo and Puig, 1984). In addition, several discontinuous
168 outcrops occur from Quebrada Chañaral to southern Carrizal Bajo (Fig. 1b).

169 Bell (1984) identified nine trace-fossil ichnogenera, which yield Ordovician to Devonian ages.
170 Moreover, Bahlburg et al. (1986) reported one conodont (Gnathodus sp.), which was attributed to
171 the Carboniferous to the east of Chañaral city. According to Berg and Baumann (1985), $^{87}Rb/^{86}Sr$
172 ratios in metasediments point to a maximum depositional age of 380 ± 59 Ma. However, more
173 recently, detrital zircons from a meta-sandstone located in the Punta de Choros Metamorphic
174 Complex yield a maximum deposition age of 334 ± 6 Ma, pointing to an overlap between the
175 sedimentary and tecto-metamorphic processes (Navarro, 2013). Bell (1987) described the presence
176 of spiriferaceans and bryozoans within limestone blocks in mélange facies of Carboniferous to
177 Permian ages.
178 The sedimentary structures and rock types indicate a deep-sea basin-plain depositional environment
179 (Bell, 1982). Las Tórtolas Formation, based on lithostratigraphic characteristic, has been correlated
180 with the Devonian to Carboniferous El Toco Formation, located to the north of Antofagasta city
181 (Garcia, 1967; Bell, 1982).
182 The Las Tórtolas Formation was defined by Godoy and Lara (1998) as the Chañaral
183 Epimetamorphic Complex, a mainly metaturbiditic quartzite-phyllite petrotectonic association,
184 including mélange facies, with a low proportions of metabasites and metalimestones.
185
186 *The Chañaral mélange*
187 The Chañaral mélange, defined as a sequence of chaotically deformed distal turbidites, is comprised
188 by identical lithologies to those of the Las Tórtolas Formation, which are differentiated by the
189 extreme dissociation and mixed layers of the former (Bell, 1982; 1984). It outcrops discontinuously
190 from south Chañaral city to Carrizal Bajo (Fig. 1a, b). The mélange facies was produced by the
191 mechanical breakdown and mixing of both unconsolidated and partly lithified sediments of the Las
192 Tórtolas Formation, as part of an accretionary wedge produced by the NE oblique underthrusting
193 beneath the western continental margin of Gondwana, probably during the Late Paleozoic (Bell,
194 1984; 1987; Balhburg, 1987a).
195 The mélange facies configuration was the result of two processes involving unlithified sediments.
196 An initial boudinage and break-up of the strata was accomplished by intrastratal movement
197 resulting from imbricate thrusting within the accretionary wedge. In the second process, the cross-
198 cutting zones of breccia, which are interpreted as fluid escape conduits resulting from the high pore
199 pressures produced during underthrusting, give rise to the breccia mélange (Bell, 1984; 1987). Bell
200 (1987) defined three deformational phases in the study area: D_1 resulted in the stratal disruption and
201 mixing which produced the mélange organization. Subsequent tectonic deformation (D_2 and D_3)
202 produced slaty and crenulation cleavages, schistosity and flattening of blocks in the mélange, which

are associated with low-grade metamorphism (Bell, 1987). Bell (1987) defined gradational contacts between the Las Tórtolas Formation and mélange in several locations to the south of Chañaral city.

3.- Rock descriptions and structural analysis

3.1 Rock descriptions and field relationships

In the study area (Fig. 1c, d), the Las Tórtolas Formation shows two main exposure areas with contrasted structural characteristics that are separated by a major structure called here Infieles fault (Fig. 1c, d; 2a, b). To the east, the metasedimentary formation is dominated by thrust faults and associated fault-propagation folds (Fig. 2c), where the quartzite-phyllite sequence shows layers of great lateral continuity and low metamorphic grade. Occasionally, quartzite layers present folded pinch and swell structures (Fig. 2d). This zone is considered as the brittle-ductile domain. To the west of the Infieles fault, the Las Tórtolas Formation is composed of the mélange facies. These are characterized by individualized quartzite blocks, with major axes ranging in length from several centimeters to tens of meters, in a phyllitic matrix (Fig. 2e). This structure is produced by the disruption of the original architecture of the turbidite succession.

The Infieles fault is a major structure, N-S to N20ºE trending and dipping to the E or ESE, with dextral-reverse fault kinematics and top-to-the-west displacement (Fig. 2a). The fault rock associated with the Infieles fault attains up to 2-5 meters in thickness to the north (Fig. 2b). In the study area, this structure crosscut various lithologies, mainly microgranular chloritized intrusives and quartzites, showing slightly cohesive to non-cohesive cataclastic textures. Several secondary thrusts or splays branch out from the main fault surface with N-S to N160E azimuth, giving place to a duplex structure, whose basal horses are composed of the mélange facies preserving the average structural orientations measured in the mélange domain (Fig. 1d). To the south (Fig. 1c), medium to high grade Crd-schists thrusted over low grade phyllites and quartzites (mineral abbreviations after Kretz, 1983). To the south of the study area, the abundance of volcanic rocks of undetermined age, and the contact aureole of the Flamenco pluton do not allow us recognizing whether the contact between the mélange facies and the brittle-ductile domain occurs through the Infieles fault or it is rather transitional.

Moreover, the Las Tórtolas Formation in both structural domains contains conglomerates, shales and pelagic cherts. These lithologies, together with quartzite blocks, crop out as strongly deformed lensoidal bodies in the mélange facies (Fig. 2f, g), whilst in the brittle-ductile domain they constitute a deformed meta-turbiditic sequence with alternating 1 to 3 m thick layers. Besides, the

237 mélange facies shows highly deformed rocks of chloritic composition (Fig. 2h), interpreted as
238 former volcanic rocks or even pillow lavas (Bell, 1982) interbedded among the rocks of the original
239 sedimentary basin. In the brittle-ductile zone, andesitic volcanic rocks consist of Pl phenocrysts and
240 rock fragments in a microgranular matrix. They show tectonic contacts with phyllites and
241 quartzites, being affected by the fold and thrust structures.
242 Petrologically, the mélange facies and the brittle-ductile domain contain similar lithologies. Both of
243 them consist of more than 90% of quartzite and phyllite of low metamorphic grade. Phyllites are
244 mostly composed of Bt in the mélange facies, and of Bt + Ms + Chl and minor amounts of Qtz and
245 feldspar in the brittle-ductile domain.
246
247 *3.2 Petrography of quartzite blocks*
248
249 *General description*
250 The analysed samples come from three different structural analysis stations (6, 14, 15; Fig. 1c).
251 Each sample has been studied through three orthogonal sections according to the orientations of the
252 main quartzite block axes (see shape preferred orientation (SPO) in chapter 4 for details). They are
253 all impure quartzites with variable amounts of white mica, iron hydroxides, biotite, feldspar and
254 opaque minerals. 6 is more impure and 14 is formed almost only by quartz. In each sample, purer
255 and more impure areas are distinguishable. In impure areas (samples from 6 and some areas of
256 samples from 15, quartz modal proportion slightly under 90 %.), quartz typically appears as
257 medium sized (0.05 to 0.5 mm), round to elliptical, sub-rectangular or irregular quartz grains (Fig.
258 3a) embedded in a fine grain (3-30 μm) matrix formed by quartz, white mica, biotite, some feldspar,
259 iron hydroxides and minor opaque minerals. In purer quartzite areas (quartz modal proportion over
260 90 %) white mica appears as the only minor phase. These fine-grained (0.01 – 0.05 mm) quartzites
261 (most from samples of station 14) are crosscut by several quartz veins (Fig. 3b) with no apparent
262 preferred direction. Modal proportion of minor phases in these veins is under 1 %. Vein thickness
263 typically ranges from 0.2 to 0.7 mm and grain size within the veins range from 0.03 to 0.3 mm. In
264 plane polarized light, the contacts between quartz veins and fine grain matrix appear sharp, but seen
265 in detail with crossed polarized light, these contacts are serrated, this suggesting that coarser grains
266 from the veins have grown into the matrix by grain boundary migration after inclusion of the vein.
267 No apparent foliation is observed in these samples and there are no differences among samples with
268 different orientations (A, B, C for each station). However, in samples from station 6, several
269 fractures with no preferred orientation crosscut the quartzite. These fractures contain iron
270 hydroxides and the areas around them seem to be enriched in this mineral (Fig. 3c), whereas areas

away from these fractures show very little iron hydroxide. When present, iron hydroxides appear in layers defining a rough foliation subparallel with the fracture to which is related. In these areas, foliation is enhanced by mica-rich layers and, occasionally, by the preferred orientation of sub-rectangular quartz grains (Fig. 3a).

Quartz microfabric

Quartz microfabric shows significant differences depending on the areas, more impure or purer quartzites, where is observed.

More impure areas. In these areas, quartz appears as rounded, elliptical, sub-rectangular or irregular grains that show no internal deformation or very little internal deformation with incipient undulose to sweeping extinction and scarce deformation bands (Fig. 3a). Some sub-rectangular grains are roughly oriented subparallel with the foliation defined by mica and hydroxide layers (Fig. 3a), thus defining an incipient shape preferred orientation (SPO) with no associated crystal preferred orientation (CPO). However, this SPO appears related to the orientation of fractures and thus possess only local, not regional, significance. In addition, enrichment of low soluble minerals (mica, hydroxides) occurs related to the long straight boundaries of these sub-rectangular quartz grains (Fig. 3a, c), and are interpreted as residual material produced by quartz dissolution.

Purer quartzite areas. Purer quartzite areas typically show bimodal grain size distributions. Coarse grains (0.2 – 0.6 mm) appear in veins or as aggregates, both surrounded by a fine grain (0.01 – 0.1 mm) matrix. From a qualitative inspection, neither SPO nor CPO are evident in these areas.

Coarse quartz aggregates are characterized by irregularly shaped grains with serrated high-angle boundaries (Fig. 3b, d, e, f). Recrystallization bulges (Fig. 3d, e) as well as few "window" and "pinning" structures are observed along these boundaries. Also, some isolated grains appear inside larger ones (Fig. 3d). The latter can be interpreted as (1) spontaneous nucleation of newly formed grains (e.g., Drury and Urai, 1990; Vernooij et al., 2006), (2) "left-over grains" (e.g., Jessell, 1987) or (3) strongly irregular bulges connected with the neighbouring grain underneath the observation surface. Main internal deformation features are undulose, patchy and sweeping extinction (Fig. 3b, d, e), deformation bands and subgrains with serrated boundaries (Fig. 3d). Finer newly recrystallized quartz grains with no or little internal deformation usually concentrate along serrated coarse grain boundaries and planar surfaces, likely fractures, inside grains (Fig. 3f).

In spite of their grain size range (0.01 – 0.1 mm), fine grains surrounding coarser grains are very uniform in size, being typically around 0.07 – 0.08 mm (Fig. 3g, h). In these areas, granoblastic textures defined by straight grain and subgrain boundaries defining 120º triple junctions coexist with irregularly shaped grains that usually bulge into slightly coarser grains (Fig. 3g, h). These

coarser grains are very irregular in shape, and show internal deformation features, such as undulose and patchy extinction and/or subgrains (Fig. 3h). Nevertheless, the crystallographic orientation of each of these irregular grains (deduced from cross-polarized images and gypsum plate inserted) suggests they are actually one single grain, likely much coarser in origin, that has been progressively reduced in size by recrystallization.

3.3 Structural description and domains

Mélange facies

The mélange facies has been defined as a chaotic mixture of quartzite blocks in a phyllitic matrix (Bell, 1982). However, in the study area, the structural analysis allows distinguishing two structural domains in the mélange facies due to the fragmentation of the original architecture of the turbidite sequence. These domains are characterized by linear (L) and linear-planar (L-S) fabrics, where the shape of the quartzite blocks corresponds to the fabric found in the phyllite matrix. The linear fabric domain is determined by the constrictional ellipsoid shape of quartzite blocks, whose long axes define the stretching lineation, and by the L-tectonites with "pencil structure" observed in the phyllite matrix, where the foliation planes are no identifiable (Fig. 4a). The L-S fabric domain is characterized by the flattening ellipsoid shape of the quartzite blocks. These flat objects show two principal lengthening directions, while the planar fabric coincides with the foliation planes observed in phyllitic S-tectonites.

Furthermore, other significant structures observed in the mélange facies are tight to isoclinal folds (Fig. 4b). The orientation of fold axes and axial planes coincide with the lineation and foliation defined in quartzite blocks and phyllite matrix, respectively. Occasionally, a spaced crenulation cleavage can be observed in phyllites (Fig. 4c). This crenulation is related to the axial planes of small kink or very angular folds. Other recognizable structures in the mélange facies are asymmetric objects (Fig. 4d), S-C structures (Fig. 4e) and the ubiquitous boudinage observed in quartzite layers and, occasionally, in syn-deformational dykes (Fig. 4f). The surfaces where the maximum asymmetry is recognized in shear structures contain the lineation and are orthogonal to the foliation. The deformation intensity prevents the accurate identification of the deformation processes responsible for the fragmentation of the original sedimentary structure. However, S-C, boudinage and pinch and swell structures are the most conspicuous throughout the study area. These structures are characteristic of shear zones and probably conditioned the formation of the mélange facies.

The tectonic foliation (S_1) is defined in the mélange by both the phyllite cleavage and the planes outlined by the long and intermedium axes of quartzite blocks. This S_1 foliation shows a constant N140º-150ºE azimuth, dipping 40º to 85º to NE and SW (Fig. 1d, 5). In the L domains, the long axes of quartzite ellipsoids and the phyllite lineations (L_1) present similar NW-SE trends, plunging 5º-20º to NW and SE. The orientation of the axes of isoclinal folds (F_1) coincides with that of L_1 lineations (Fig. 5). Crenulation cleavages (S_2) show N150º-160ºE azimuths, dipping to the NE, which are similar to the statistical F_2 axial planes (Fig. 5). At a large, cartographic scale, F_2 folds are close to tight, moderately inclined chevron folds, which are denoted by the absence of gently dipping foliations. Small kink folds associated with the generation of S_2 represent F_2 folding at a mesoscopic scale.

Brittle-ductile domain

The structure in the brittle-ductile domain is determined by the primary foliation planes defined by the contacts between phyllite and quartzite layers, corresponding to the original sedimentary contacts in the turbiditic sequence (S_0). Quartzite bands show a great lateral continuity and variable thickness, from decimeters to several meters. However, in several locations, boudinage and pinch and swell structures are observed. Although the quartzite layers were not fragmented by this stretching phase, it clearly generated necking structures (Fig. 2h). These structures are previous to those resulting from the subsequent thrusting and related folding phase that affected the S_0 planes. Southwest vergent inclined folds are associated with the propagation of imbricate, N160ºE trending thrusts (Fig. 1d). A highly penetrative foliation developed in phyllite layers (S_1), axial plane to the fold train. These map-scale folds are mainly recognized by the normal-overturned limb succession, albeit some hinges can be observed (Fig. 2d). The statistical axial planes adscribed to F_1 folding in the brittle-ductile domain are oriented about N165ºE/30ºNE, resulting in gently inclined, SW vergent folds (Fig. 5). The S_0 and S_1 orientation dispersion observed in the spherical plots (Fig. 5) might be adscribed two a subsequent N60º-70ºE trending folding (F_2) that affected the thrust planes and associated folds in this area.

4.- SPO determination

In order to study the shape preferred orientation (SPO) in the mélange facies, 18 sampling stations were chosen along the study area (Fig. 1c). Mesoscopic SPO has been analysed in quartzite blocks and the lengths of the main axes of the ellipsoidal bodies have been directly measured in the

372 stations, with the aim to obtain aspect ratios and the shape parameter of Flinn (1962) (Table 1). One
373 representative quartzite object has been analysed in each station.
374 SPO in Qtz microfabric has been determined in the samples used for the mesoscopic study. For this,
375 we have obtained three orthogonal oriented sections from quartzite bodies (Fig. 6a). High-resolution
376 digital images were taken with an optical microscope at the studied sections and edited with
377 Photoshop_ and ImageJ editor software to emphasize quartz grains and textures, reduce image noise
378 and to create a grey scale image file. Each of the images is oriented and represents a principal plane
379 of the ellipsoids formed by quartzite blocks (Fig. 6b). These sections and their orientations have
380 been introduced in the SPO and Ellipsoid software (Robin, 2002; Launeau and Robin, 2005) to
381 obtain the shape ratio and the long axis orientation of the sectional fabric ellipses (Fig. 6c), and the
382 three-dimensional ellipsoid data (Fig. 6d) respectively. The Ellipsoid output includes the orientation
383 and the normalized length of each principal axis (Fig. 6d, Table 2). These results are plotted beside
384 the location of the station in Figure 7a.
385
386 *4.1 SPO determination in quartzite blocks*
387 According to the Flinn shape parameters resulting from the measurement of quartzite blocks (Table
388 1, Fig. 7b), only station 1 shows an apparent flattening fabric ellipsoid (shape parameter = 0.5).
389 Stations 3, 4, 7, 9, 10 and 12 yielded parameters between 1 and 1.5, which corresponds to
390 approximately plane strain shape ellipsoids. The remaining stations show Flinn shape parameters
391 greater than 1.5, being thus located in the apparent constriction field. These results coincide with the
392 field observations presented in Figure 5. Stations 17 and 18 show almost continuous quartzite
393 layers, which hinders the estimation of the axis lengths of the measured blocks. Thereby, the
394 mélange area is partitioned between a linear fabric domain (L), where constrictional quartzite-block
395 shape ellipsoids have been determined, and a linear-planar fabric domain (L-S), where plane-strain
396 or flattening quartzite-block shape ellipsoid are obtained by means of mesoscopic axes
397 measurement.
398
399 *4.2 SPO determination in quartz microfabric*
400 Table 2 shows the SPO results obtained in quartz microfabric using SPO and Ellipsoid softwares
401 (Robin, 2002; Launeau and Robin, 2005). Results include a calculated foliation, axes orientations
402 and normalized values, aspect ratios, and Flinn, intensity (Nadai, 1950) and shape (Lode, 1926)
403 parameters. Normalized standard deviations around the mean (parameter of Robin, 2002) are
404 between 2 and 18%.

405 Stations 5, 6, 12 and 13 show the highest Flinn shape parameters (>1.5) for quartz microfabric,
406 which correspond to apparent constrictional ellipsoids. Samples 1, 2, 3, 8, 15, 17 and 18 are very
407 close to K=1 (Flinn logarithmic shape parameter), indicative of plane strain ellipsoids, whilst
408 stations 4, 7, 9, 10, 11 and 14 present Flinn shape parameters lower than 0.5 and are located in the
409 apparent flattering field in Flinn's diagram. However, all samples except 6 are very close to the
410 origin, suggesting a significatively low degree of development of the SPO. It is noteworthy that
411 aspect ratios are considerably lower than the values obtained from the mesoscopic fabric. Besides,
412 calculated foliations do not coincide in most stations with field measurements (Fig. 7a).
413
414
415 **5.- Discussion**
416
417 The structural characteristics of the study area allow us to organize the multistage deformation
418 history recorded in the Chañaral mélange, and to assess the processes that configure the mélange
419 facies in different structural domains.
420 The observed mélange facies are produced by the complete disruption of the original architecture of
421 the turbidite succession. From a structural point of view, mélange ductile deformation could be
422 related to a mylonitic shear zone. Indeed, in the present study and as discussed below, we interpret
423 the textures of the mélange as the result of a deformational process driven by the activity of a shear
424 zone, and not as a syn-depositional texture which is further subjected to a tectonic deformation
425 process (Bell, 1987). However, the rheological framework of the sedimentary rocks subjected to
426 this deformation is critical to understand the final disposal of mélange tectonic fabrics.
427 An essential observation to account for the correspondence between the disrupting process of the
428 sedimentary sequence and the tectonic fabrics is the relation between the mesoscopic shape of
429 quartzite blocks and the fabrics developed in the phyllitic matrix. Where quartzite bodies show a
430 prolate shape, L-tectonites are present in the phyllite matrix, corresponding with a constrictive
431 deformation. These areas have been referred to as L domains (Fig. 5). Where quartzite blocks
432 exhibit a flattened shape, and two obvious stretching directions are present, a planar fabric
433 dominates the phyllitic matrix. These typical flattening rocks are labelled L-S domains. The most
434 common mechanism that acted in the mélange to yield the described structural configuration is
435 boudinage (Fig. 2, 4), in addition to heterogenous shearing (S-C structures, Fig. 4e) and folding
436 processes that generated intra-foliation tight to isoclinal folds (Fig. 4b). The arrangement of the L_1
437 and S_1 fabrics (Fig. 5), together with some scarce asymmetric structures, indicate a predominant
438 NW-SE-directed dextral shearing. These structures have been ascribed to a first deformation phase,

439 D_1. In turn, the S_1 foliation describes map-scale chevron folds (F_2) responsible for its high dipping
440 angles. This is consistent with the folding morphologies expected for the high mélange viscosity
441 contrast between the quartzite blocks and the phyllitic matrix (Ramsay and Huber, 1987). The
442 variable plunging of L_1 lineations might be caused by F_2 folds (Fig. 5).
443 In the brittle-ductile domain, to the east of the Infieles fault, the folds affecting the continuous
444 layers of the quartzite-phyllite sequence are related to N160º-165ºE trending thrust faults. These
445 folds developed a NE dipping penetrative axial-plane foliation in phyllite layers (Fig. 2c, d and 5).
446 Thrusting duplexes and associated folds are typical of accretionary prisms during the underplating
447 of subduction mélanges (McClay, 1981; Davis et al., 1983; Escuder-Viruete and Baumgartner,
448 2014). The boudinage of competent layers (quartzites) observed in the brittle-ductile domain of the
449 Las Tórtolas Formation (Fig. 2d) might be caused by a previous phase of basal accretion, shear-
450 thinning flow regime and a horizontal extension into the prism (Feehan and Brandon, 1999; Richter
451 et al, 2007). Both major chevron and inclined fault-propagation folds observed in the mélange and
452 brittle-ductile domains respectively show similar orientations (thrust-associated folds are slightly
453 more northernly directed) and vergences, therefore they could be related to the same tectonic event
454 (D_2), in areas belonging to different tectono-structural domains.
455 A third deformational phase (D_3) affected the axial traces of D_2 folds in the brittle-ductile zone
456 although this is not clearly shown in the mélange facies.
457 Bell (1987) described the formation of mélange textures in the Chañaral mélange as a process of
458 stratal breakup of unconsolidated sediments followed by brecciation produced by hydraulic
459 fracturing. Subsequent tectonic deformation phases would be responsible for the observed foliations
460 and crenulations, whose orientations and vergences coincide with those described in this study.
461 However, the correlation between the constrictional and flattened shape of quartzite objects and the
462 L and L-S tectonites found in their phyllite matrix, points to a tectonic deformation (D_1) as the
463 process that promoted the generation of the mélange textures during the obliteration of the original
464 turbiditic sequence. This does not preclude the presence of fluid-scape structures favoured by the
465 possible incomplete consolidation of sediments and their high water contents.
466 Other examples of tectonic mélange formations associated with active continental margins have
467 been interpreted as due to strong ductile deformation (i. e., Shi et al, 2013; Escuder-Viruete and
468 Baumgartner, 2014), and not to syn-sedimentary processes of gravitational collapse or
469 olistostromes. These tectonic mélanges include structures as boudins, features due to plastic flow,
470 stacking folds and thrust duplexes among others, as well as a succession of deformational phases of
471 positive tectonic inversion (Williams et al., 1989), similar to those described in this study.

One of the most significant results of this study is the observation of the deformation partitioning between a ductile deformation zone (mélange facies) and a brittle-ductile zone in the Las Tórtolas Formation, limited by a map-scale structure (Infieles fault). Furthermore, the mélange facies shows two structural domains characterized by linear (L) and planar-linear (L-S) fabrics. The study of SPO measured in mesoscopic quartzite blocks coincides with these observations. The higher values of K, and therefore the shape ellipsoids located in the constrictive field, are found in L domains (Fig. 7b), while quartzite bodies measured in L-S domains yield Flinn shape parameters close to K=1 (Table 1). The intensity of deformational process is reflected in the high aspect ratios yielded by the quartzite ellipsoidal block axes (Fig. 7b).

Regarding the microstructures observed in more impure quartzite areas, such as sub-rectangular, low strained, grains with enrichment of low soluble minerals along straight boundaries (Fig. 3a, c) point to dissolution-precipitation creep (Trepmann et al., 2010 and references therein) as the principal deformation mechanism in these areas. This mechanism is typically active at HP/LT (ca. 350 ºC) deformation at low differential stresses (Trepmann and Stöckhert, 2009; Grigull et al., 2012). On the other hand, the texture observed in purer quartzite areas, with bimodal grain size distributions (Fig. 3e), can be loosely regarded as core-and-mantle structures (Stipp et al., 2002). Irregularly shaped grains and subgrains along grain boundaries and fractures inside coarse grains (Fig. 3f) are interpreted as new grains formed by bulging recrystallization (Bailey and Hirsch, 1962; Drury et al., 1985; Drury and Urai, 1990; Stipp et al., 2002; Vernooij et al., 2006), which involves mainly slow grain boundary migration although normally assisted by subgrain rotation (Bailey and Hirsch, 1962; Means, 1981; Tungatt and Humphreys, 1984; Drury et al., 1985; Urai et al., 1986; Stipp et al., 2002). “Window” and “pinning” structures as well as “left-over grains” also suggest grain boundary migration (Jessell, 1987). On the other hand, matrix strain-free grains occasionally show granoblastic textures with very weak associated CPO, although they do not overgrow late fractures. These features are indicative of very limited static recrystallization (e.g., Trepmann et al., 2010). Therefore, it is likely that in the purer quartzite areas, quartz deformed between the upper part of the bulging recrystallization regime and its transition to the subgrain rotation regime, which would yield a temperature between 340 and 400 ºC (Stipp et al., 2002). Late subordinate static recrystallization could have been occurred, perhaps in relation to deformation at very low-stress in an accretionary complex (Trepmann et al., 2010).

Irrespective of the deformation mechanism invoked in the studied samples (bulging-subgrain rotation recrystallization and dissolution-precipitation creep), the deduced temperature is in the range between 350 – 400 ºC, which coincides with the greenschists facies metamorphism proposed for the Las Tórtolas Formation and the mélange facies (Miller 1970; Aguirre et al. 1972, Bell,

506 1987), and are slightly higher than those estimated by Marioth and Bahlburg (2003) (300-350 °C) in
507 metapelites of the Chañaral mélange. This temperature range matches that obtained from
508 blueschists and greenschists present in Western Series during the high-pressure metamorphism
509 episode (Willner, 2005). The question is how these two different deformation mechanisms
510 coexisted? It is suggested (e.g., Trepman et al., 2010) that dissolution-precipitation creep activates
511 only when differential stress is too low to activate dislocation creep, which is necessary to produce
512 dynamic recrystallization. In any case, the presence of a fluid is also necessary (e.g., Rutter, 1976).
513 In the studied samples, microstructures suggesting dissolution-precipitation creep are evident
514 mainly in more impure quartzite areas, which are normally located around large fractures.
515 Therefore, it is hypothesized that in the studied samples, purer quartzite areas are fluid-free and are
516 thus deformed mainly by bulging dynamic recrystallization. In contrast, in more impure areas,
517 dissolution-precipitation creep was favoured by the presence of fluids transported along fractures.
518 It has been shown that D_1 mesoscale structures, foliation and, particularly, lineation, are very
519 conspicuous. They are defined by a strong SPO displayed by the quartzite lenses and by the
520 phyllites that surround them. In contrast, the microstructure of the quartzite lenses does not show
521 evidences for intense deformation: there are no apparent foliations or lineations, fractures and
522 quartz veins appear as planar non-deformed structures, quartz aggregates do not show elongated
523 ribbons, nor intense SPO (Fig. 7) or CPO. From the microstructure analysis, it is likely that D_1
524 deformation within the quartzite lenses took place mainly via bulging recrystallization and
525 dissolution-precipitation creep. It is likely that these striking differences between meso- and
526 microstructures can be assigned to a process of dissolution-precipitation creep at the outcrop scale.
527 Quartzite lenses can behave as high viscosity bodies embedded in a less viscous material
528 represented by the phyllites. As such, dissolution occured at high differential stress boundaries of
529 the quartzite layers and precipitation at low differential stress parts (strain shadows related to these
530 bodies). This would have increased the aspect ratio of the lenses favouring the development of the L
531 tectonites whereas internally, these quartz lenses would have remained virtually unstrained. A
532 similar process is proposed by Grigull et al. (2012) for comparable block-in-matrix structures of
533 tectonic mélanges related to subduction channels.
534 With regard to the age of the deformational process, an update of the geochronology can be attained
535 through the relationship between the deformation phases and the syn- to post-intrusive igneous
536 rocks. For this purpose, an upper limit for the age of the mélange facies generation should be set at
537 the time of the Late Triassic to Early Jurassic magmatic arc emplacement (i. e., Charrier et al.,
538 2007; Grocott and Taylor, 2002; Kato and Godoy, 2015), hosted in the Las Tórtolas Formation,
539 including mélange facies. Younger middle Permian ages have been proposed by García-Sansegundo

et al. (2014) for the onset of the subduction in the current South American continental margin. At this time, those rocks related to the accretionary complex became part of the arc, which suggests the displacement of the accretionary complex to the east.

Figure 8 proposes a model for generating mélange facies in northern Chile and its relationship to the structural domains described in the Las Tórtolas Formation, based on the known dynamics of the western active margin of Gondwana between the Late Paleozoic to Jurassic (Mpodozis and Ramos, 1989; Mpodozis and Kay, 1992; Mpodozis and Ramos, 2008). During the Late Paleozoic, the fast convergence enables the development of an extensive accretionary complex (Mpodozis and Ramos, 1989), and the high availability of sediments in the subduction channel, dominated by quartzitic and pelitic lithologies, with lowest proportion of oceanic crust rocks (Fig. 8a, b), where the structures and deformation partitioning described in this study are generated (D_1 deformational phase). However, in central Chile (Pichilemu region), N- to E-MORB derived amphibolites have been described as part of the oceanic crust accreted to the active margin (Hyppolito et al., 2014a).

The accretion of exotic terranes to the continental margin during the Late Permian to Triassic (Equis terrane; Mpodozis and Kay, 1992) displaced the Paleozoic accretionary complex to the east, promoting a transition to a brittle-ductile deformation that affected to the mélange rocks, and the folding and verticalization of the previous structures (D_2 deformational phase) (Fig. 8c, d). D_2 phase might be contemporary or immediately prior to the formation of high-angle, N-S trending brittle-ductile to brittle shears described by Kato and Godoy (2015). A similar deformational phase sequence is described by García-Sansegundo et al. (2014) in the Choapa Metamorphic Complex (central Chile), where the HP-LT subduction-related D1 episode is followed by the exhumation and obduction process (D2) caused by the arrival of oceanic reliefs, attributed to X terrane, at the subduction zone.

Finally, during the subduction reactivation in the Early Jurassic (Mpodozis and Ramos, 2008), crustal extensional tectonics favoured the emplacement of cordilleran granitoids and the building of the Jurassic-Cretaceous magmatic arc, hosted by the metasediments of the Paleozoic accretionary complex, called the Las Tórtolas Formation, including the Chañaral mélange (Fig. 8e).

6.- Conclusions

This structural analysis is part of an ongoing study about the mélange facies within the Paleozoic basement of the Coastal Range batholith in northern Chile. The addresing problems to figure out are the tectonic setting of the mélange facies, the age of the deformational process and the mechanisms

of deformation partitioning between the flattening and constriction domains. This study hypothesizes with the conformation of two structural domains in the Chañaral mélange due to the rheological framework of unconsolidated or poorly consolidated sediments, their fluid contents and the variation of differential stress during the motion of the intensely deformed mélange facies. However, in future work advances, other possibilities such as the presence of a transtensive context with variations in the vorticity values and in the intensity of the internal deformation must be considered.

The mélange facies shows lithologies and textures that can be related to subduction channels, with a predominance of phyllites and quartzites (up to 90%) and minor amounts of limestones, conglomerates, cherts and retrograded basaltic rocks. However, the absence of high-pressure rocks, which are described in the Late Paleozoic mélange formations in central Chile, and the greenschist metamorphism measured in the Chañaral mélange, locate these mélange facies in a low temperature zone of the subduction channel, without the presence of deep upward flows that provide rocks from high pressure areas. This might be related to the fast convergence and the availability of sediments in the subduction channel, which activate the processes of frontal and basal accretion during Late Paleozoic. The subsequent terrane accretion drives the subduction axis to the west, and promotes the intensive folding of the mélange facies. This finally configures the Las Tórtolas Formation as the basement of the Andean Jurassic-Cretaceous magmatic arc in northern Chile.

Acknowledgments

This work has been developed during the PhD Thesis proposal of Paulina Fuentes, carried out at the Department of Geology of the University of Atacama. The work was funded with FONDECYT Project Nº 11140722 of CONICYT, and with the fund support of DIUDA 2013-22268 and DIUDA 2014-22273 projects. We are grateful for constructive colleague reviews by Enrique Bernárdez and Wolfgang Griem, all of which improved the manuscript.

References

Abbate, E., Bortolotti, V., Passerini, P., 1970. Olistostromes and olistoliths. Sedimentary Geology 4, 521–557.

608 Aguirre, L., Hervé, F., Godoy, E., 1972. Distribution of metamorphic facies in Chile—an outline.
609 Krystallinikum 9, 7-19.
610
611 Arévalo, C., Grocott, J., 1997. The tectonic setting of the Chañarcillo Group and the Bandurrias
612 Formation: An Early-Late Cretaceous sinistral transpressive belt between the Coastal Cordillera and
613 the Precordillera, Atacama region, Chile: Congreso Geológico Chileno, 8th, Antofagasta,
614 1997. Actas 3, 1604-1607.
615
616 Bahlburg, H., 1987. Sedimentology, petrology and geotectonic significance of the Paleozoic flysch
617 in the Coastal Cordillera of northern Chile. Neues Jahrbuch für Geologie und Paläontologie
618 Monatshefte 1987, 527-559.
619
620 Bahlburg, H., Breitkreuz, C., Zeil, W., 1986. Paläozoische Sedimente Nordchiles. Berliner Geowiss
621 Abh A 66, 147-168.
622
623 Bailey, J.E., Hirsch, P.B., 1962. The recrystallization process in some polycrystalline metals.
624 Proceeding of the Royal Society of London A267, 11-30.
625
626 Bell, C.M., 1982. The Lower Paleozoic metasedimentary basament of the coastal ranges of Chile
627 between 25°30' and 27°S. Revista Geológica de Chile 17, 21-9.
628
629 Bell, C.M., 1984. Deformation produced by the subduction of a Paleozoic turbidite sequence in
630 northern Chile. Journal of the Geological Society of London 141, 339-47.
631
632 Bell, C.M., 1987. The origin of the Upper Palaeozoic Chanaral mélange of N Chile. Journal of the
633 Geological Society of London 144, 599–610.
634
635 Berg, K., Baumann, A., 1985. Plutonic and metasedimentary rocks from the Coastal Range of
636 northern Chile: RbSr and UPb isotopic systematics. Earth and Planetary Science Letters 75, 101–
637 115.
638
639 Bettelli, G., Vannucchi, P., 2003. Structural style of the offscraped Ligurian oceanic sequences of
640 the Northern Apennines: new hypotesis concerning the development of mélange block-in-matrix
641 fabric. Journal of Structural Geology 25, 371–388.

642
643 Bortolotti, V., Cortesogno, L., Gaggero, L., Lahondere, D., Marroni, M., Molli, G., Montanini, A.,
644 Pandolfi, L., Prinicpi, G., Rossi, P., Saccano, E., Treves, B., Tribuzio, R., 2004. Northern Apennine
645 and Corsica ophiolites: The oceanic lithosphere of the ligure-piemontese basin and its transition to
646 the Adria continental margin (Italy). Memorie Descrittive della Carta Geologica d'Italia 63, 1–12.
647
648 Brandon, M.T., Calderwood, A.R., 1990. High-pressure metamorphism and uplift of the Olympic
649 subduction complex. Geology 18 (12), 1252-1255.
650
651 Byrne, T., 1994. Sediment deformation, dewatering and diagenesis: illustrations from selected
652 mélange zones. In: Maltman, A. (Ed.), Geological deformation of sediments. Chapman and Hall,
653 pp. 239–260.
654
655 Camerlenghi, A., Pini, G.A., 2009. Mud volcanoes, olistostromes and Argille scagliose in the
656 Mediterranean region. Sedimentology 56, 319–365.
657
658 Castro, A., Gerya, T., García-Casco, A., Fernández, C., Díaz Alvarado, J., Moreno-Ventas, I.,
659 Loew, I., 2010. Melting relations of MORB-sediment mélanges in underplated mantle wedge
660 plumes. Implications for the origin of cordillerantype batholiths. Journal of Petrology 51, 1267-
661 1295.
662
663 Castro, A., Vogt, K., Gerya, T.V., 2013. Generation of new continental crust by sublithospheric
664 silicic-magma relamination in arcs: a test of Taylor's andesite model. Gondwana Research 23,
665 1554-1556.
666
667 Cawood, P.A., Kröner, A., Collins, W.J., Kusky, T.M., Mooney, W.D., Windley, B.F., 2009.
668 Accretionary orogens through Earth history. Geological Society, London, Special Publications 318
669 (1), 1-36.
670
671 Charrier, R., Pinto, L., Rodriguez, M.P., 2007. Tectonostratigraphic evolution of the Andean
672 Orogen in Chile. In: Moreno, T., and Gibbons, W., (Eds.), The geology of Chile: Geological
673 Society of London, pp. 1–114.
674

675 Cloos, M., 1982. Flow mélanges: numerical modeling and geologic constraints on their origin in the
676 Franciscan subduction complex, California. Geological Society of America Bulletin 93, 330–345.
677
678 Cloos, M., Shreve, R.L., 1988. Subduction-Channelmodel of prismaccretion,mélange formation,
679 sediment subduction, and subduction erosion at convergent platemargins: 1. Background and
680 description. Pure and Applied Geophysics 128 (3–4), 455–500.
681
682 Condie, K.C., 2007. Accretionary orogens in space and time. Geological Society of America
683 Memoirs 200, 145-158.
684
685 Cousineau, P.A., 1998. Large-scale liquefaction and fluidization in the Cap Chat Mélange, Quebec
686 Appalachians. Canadian Journal of Earth Sciences 35 (12), 1408–1422.
687
688 Cowan, D.S., 1985. Structural styles in Mesozoic and Cenozoic mélanges in the western Cordillera
689 of North America. Geological Society of America Bulletin 96, 451–462.
690
691 Davis, D., Suppe, J., Dahlen, F.A., 1983. Mechanics of fold-and-thrust belts and accretionary
692 wedges. Journal of Geophysical Research 88 (B2), 1153-1172.
693
694 Deckert, H., Ring, U., Mortimer, N., 2002. Tectonic significance of Cretaceous bivergent
695 extensional shear zones in the Torlesse accretionary wedge, central Otago Schist, New
696 Zealand. New Zealand. Journal of Geology and Geophysics 45(4), 537-547.
697
698 Dilek, Y., Imamverdiyev, N., Altunkaynak, S., 2010. Geochemistry and tectonics of Cenozoic
699 volcanism in the Lesser Caucasus (Azerbaijan) and the peri-Arabian region: Collision-induced
700 mantle dynamics and its magmatic fingerprint. International Geology Review 52, 536–578.
701
702 Drury, M.R., Urai, J.L., 1990. Deformation-related recrystallization processes. Tectonophysics 172,
703 235-253.
704
705 Drury, M.R., Humphreys, F.J., White, S.H., 1985. Large strain deformation studies using
706 polycrystalline magnesium as rock analogue. Part II: dynamic recrystallization mechanisms at high
707 temperatures. Physics of the Earth and Planetary Interiors 40, 208-222.
708

709 Escuder-Viruete, J., Baumgartner, P.O., 2014. Structural evolution and deformation kinematics of a
710 subduction-related serpentinite-matrix mélange, Santa Elena peninsula, northwest Costa
711 Rica. Journal of Structural Geology 66, 356-381.
712
713 Federico, L., Crispini, L., Scambelluri, M., Capponi, G., 2007. Ophiolite mélange zone records
714 exhumation in a fossil subduction channel. Geology 35, 499–502.
715
716 Feehan, J.G., Brandon, M.T., 1999. Contribution of ductile flow to exhumation of low-temperature,
717 high-pressure metamorphic rocks: San Juan-Cascade nappes, NW Washington State. Journal of
718 Geophysical Research: Solid Earth 104 (B5), 10883-10902.
719
720 Festa, A., Dilek, Y., Pini, G.A., Codegone, G., Ogata, K., 2012. Mechanisms and processes of
721 stratal disruption and mixing in the development of mélanges and broken formations: Redefining
722 and classifying mélanges. Tectonophysics 568, 7-24.
723
724 Festa, A., Pini, G.A., Dilek, Y., Codegone, G., 2010. Mélanges and mélange-forming processes: a
725 historical overview and new concepts. In: Dilek, Y. (Ed.), Alpine Concept in Geology International
726 Geology Review 52 (10–12), 1040–1105.
727
728 Flinn, D., 1962. On folding during three dimensional progressive deformation. Quarterly Journal of
729 the Geological Society, London 118, 385-428.
730
731 García, F., 1967. Geología del norte grande de Chile. Sociedad Geológica de Chile, Santiago, Chile,
732 138 p.
733
734 García-Sansegundo, J., Farias, P., Heredia, N., Gallastegui, G., Charrier, R., Rubio-Ordóñez, A.,
735 Cuesta, A., 2014. Structure of the Andean Palaeozoic basement in the Chilean coast at 31º 30' S:
736 Geodynamic evolution of a subduction margin. Journal of Iberian Geology 40 (2), 293-308.
737
738 Godoy, E., Lara, P.L., 1998. Hojas Chañaral y Diego de Almagro, Región de Atacama. Servicio
739 Nacional de Geología y Minería, Mapas Geólogicos, no. 5-6, 1 mapa escale 1:100 000, Santiago.
740
741 Godoy, E., Welkner, D., 2003. El basamento de la costa del norte chico, chile, 20 años después. In
742 Congreso Geológico Chileno, 10th, Concepción, 2003.

Grigull, S., Krohe, A., Moos, C., Wassmann, S., Stöckhert, B., 2012. "Order from chaos": A field-based estimate on bulk rheology of tectonic mélanges formed in subduction zones. Tectonophysics 568, 86-101.

Grocott, J., Taylor, G. K., 2002. Magmatic arc fault systems, deformation partitioning and emplacement of granitic complexes in the Coastal Cordillera, north Chilean Andes (25 30′ S to 27 00′ S). Journal of the Geological Society 159 (4), 425-443.

Hervé, F., Calderón, M., Fanning, C.M., Pankhurst, R.J., and Godoy, E., 2013. Provenance variations in the Late Paleozoic accretionary complex of central Chile as indicated by detrital zircons. Gondwana Research 23, 1122–1135.

Hervé, F., Faundez, V., Calderón, M., Massone, H.-J., and Willner, A.P., 2007. Metamorphic and plutonic basement complexes. In Moreno, T., and Gibbons, W., eds., The Geology of Chile, London Geological Society, 5–19.

Hervé, F., 1988. Late Paleozoic subduction and accretion in Southern Chile. Episodes 11 (3), 183-188.

Hsü, K.J., 1968. Principles of mélanges and their bearing on the Franciscan-Knoxville Paradox. Geological Society of America Bullettin 79, 1063–1074.

Hyppolito, T., Juliani, C., García-Casco, A., Meira, T.V., Bustamante, A., Hervé, F., 2014a. The nature of the Paleozoic oceanic basin at the southwesternmargin of Gondwana and implications for the origin of the Chilenia terrane (Pichilemu region, central Chile). International Geology Review 56, 1097–1121.

Hyppolito, T., García-Casco, A., Juliani, C., Meira, T.V., Bustamante, A., Hall, C., 2014b. Late Paleozoic onset of subduction and exhumation at the western margin of Gondwana (Chilenia Terrane): Counterclockwise P–T paths and timing of metamorphism of deep-seated garnet–mica schist and amphibolite of Punta Sirena, Coastal Accretionary Complex, central Chile (34° S). Lithos 206–207, 409–434

777 Jessell, M.W., 1987. Grain-boundary migration microstructures in a naturally deformed quartzite.
778 Journal of Structural Geology 9, 1007-1014.
779
780 Kato, T.T., Godoy, E., 2015. Middle to late Triassic mélange exhumation along a pre-Andean
781 transpressional fault system: coastal Chile (26°–42° S). International Geology Review 57 (5-8),
782 606-628.
783
784 Kretz, R., 1983. Symbols for rock-forming minerals. American mineralogist 68 (1-2), 277-279.
785
786 Lash, G.G., 1987. Diverse mélanges of an ancient subduction complex. Geology 15, 652–655.
787
788 Launeau, P., Robin, P.Y.F., 2005. Determination of fabric and strain ellipsoids from measured
789 sectional ellipses—implementation and applications. Journal of Structural Geology 27 (12), 2223-
790 2233.
791
792 Lode, W., 1926. Versuche über den Einfluß der mittleren Hauptspannung auf das Fließen der
793 Metalle Eisen, Kupfer und Nickel. Zeitschrift für Physik 36 (11-12), 913-939.
794
795 Maltman, A.J., Bolton, A., 2003. How sediments become mobilized. Geological Society of London
796 Special Publications 216, 9–20.
797
798 Marioth, R., Bahlburg, H., 2003. Characterisation and quantification of thermal and diagenetic
799 processes in the Carboniferous accretionary prism (Chañaral Mélange) in northern Chile. IGCP 436
800 Final Symposium: Evolution of the Gondwana margin. In X Congreso Geológico Chileno, Actas.
801
802 McClay, K.R., 1981. What is a thrust? What is a nappe?. In: McClay. K.R. and Price, N.J. (Eds.),
803 Thrust and Nappe Tectonics. Geological Society of London Special Publication 9, 7-12.
804
805 Means, W.D., 1981. The concept of steady-state foliation. Tectonophysics 81, 179-200.
806
807 Miller, H., 1970. Vergleichende Studien an prämesozoischen Gesteine Chile unter besonderen
808 Berücksichtigung ihrer Kleintektonik. Geotektonische Forschungen 36, 1-64.
809

Mortimer, N., 1993. Jurassic tectonic history of the Otago schist, New Zealand. Tectonics 12 (1), 237-244.

Mpodozis, C., Ramos, V.A., 1989. The Andes of Chile and Argentina. In Ericksen, G.E., Cañas M.T., Reinemund, J.A. (eds.). Geology of the Andes and its relation to hydrocarbon and mineral resources, Circum-Pacific Council for Energy and Mineral Resources, Earth Science Series 11, 59-90.

Mpodozis, C., Kay, S.M., 1992. Late Paleozoic to Triassic evolution of the Gondwana margin: evidence from Chilean Frontal Cordillera batholits (28º S to 31º S). Geological Society of America Bulletin 104, 999-1014.

Mpodozis, C., Ramos, V.A., 2008. Tectónica jurásica en Argentina y Chile: extensión, subducción oblicua, rifting, deriva y colisiones?. Revista de la Asociación geológica Argentina 63 (4), 481-497.

Nádai, A., 1950. Theory of Flow and Fracture of Solids, v. 2.

Naranjo, J.A., Puig, Á., 1984. Hojas Taltal y Chañaral. Carta Geológica de Chile 62-63, 1-140.

Navarro, J.M., 2013. Petrotectónica del Complejo Metamórfico Punta de Choros, III-IV Región, Chile. Graduated thesis. University of Chile, 110 pp.

Niwa, M., 2006. The structure and kinematics of an imbricate stack of oceanic rocks in the Jurassic accretionary complex of Central Japan: An oblique subduction model. Journal of Structural Geology 28 (9), 1670–1684.

Ohsumi, T., Ogawa, Y., 2008. Vein structures, like ripple marks, are formed by shortwavelength shear waves. Journal of Structural Geology 30 (6), 719–724.

Pini, G.A., 1999. Tectonosomes and olistostromes in the Argille Scagliose of the Northern Apennines, Italy. Geological Society of America Special Papers 335, 73 pp.

Ramos, V., 1999. Plate tectonic setting of the Andean Cordillera. Episodes 22, 183-190.

Ramsay, J.G., Huber, M.I., 1987. The Techniques of the Modern Structural Geology, Volume 2: Folds and Fractures. Academic Press, London.

Raymond, L.A., 1984. Classification of mélanges. In: Raymond, L.A. (Ed.), Mélanges: Their nature, origin and significance. Boulder, Colorado. Geological Society of America Special Papers 198, 7–20.

Richter, P.P., Ring, U., Willner, A.P., Leiss, B., 2007. Structural contacts in subduction complexes and their tectonic significance: the Late Palaeozoic coastal accretionary wedge of central Chile. Journal of the Geological Society 164 (1), 203-214.

Robin, P.Y.F., 2002. Determination of fabric and strain ellipsoids from measured sectional ellipses—theory. Journal of Structural Geology 24 (3), 531-544.

Rutter, E.H., 1976. The kinetics of rock deformation by pressure solution. Philosophical Transactions of the Royal Society of London, Series A 283, 203–219.

Shi, Y., Yu, J.H., Santosh, M., 2013. Tectonic evolution of the Qinling orogenic belt, Central China: new evidence from geochemical, zircon U–Pb geochronology and Hf isotopes. Precambrian Research 231, 19-60.

Shreve, R.L., Cloos, M., 1986. Dynamics of sediment subduction, mélange formation, and prism accretion. Journal of Geophysical Research 91, 10229–10245.

Silver, E.A., Beutner, E.C., 1980. Mélanges. Geology 8, 32–34.

Stipp, M., Stünitz, H., Heilbronner, R., Schmid, S.M., 2002. The eastern Tonale fault zone: a "natural laboratory" for crystal plastic deformation of quartz over a temperature range from 250 to 700 ºC. Journal of Structural Geology 24, 1861-1884.

Taira, A., Byrne, T., Ashi, J., 1992. Photographic atlas of an accretionary prism: Geological structures of the Shimanto Belt, Japan: Tokyo, Springer-Verlag and University of Tokyo Press, 124 pp.

878 Talbot, C.J., von Brunn, V., 1989. Mélanges, intrusive and extrusive sediments, and hydraulic arcs.
879 Geology 17, 446–448.
880
881 Trepmann, C.A., Stöckhert, B., 2009. Microfabric of folded quartz veins in metagreywackes:
882 dislocation creep and subgrain rotation at high stress. Journal of Metamorphic Geology 27, 555-
883 570.
884
885 Trepmann, C.A., Lenze, A., Stöckhert, B., 2010. Static recrystallization of vein quartz pebbles in a
886 high-pressure – low-temperature metamorphic conglomerate. Journal of Structural Geology 32,
887 202-215.
888
889 Tungatt, P.D., Humphreys, S.J., 1984. The plastic deformation and dynamic recrystallization of
890 polycrystalline sodium nitrate. Acta Metallurgica 32, 1625-1635.
891
892 Ujiie, K., 2002. Evolution and kinematics of an ancient decollement zone, mélange in the Shimanto
893 accretionary complex of Okinawa Island, Ryukyu Arc. Journal of Structural Geology 24, 937–952.
894
895 Urai, J.L., Means, W.D., Lister, G.S., 1986. Dynamic recrystallization of minerals. In: Hobbs, B.E.,
896 Heard, H.C. (Eds.), Mineral and Rock Deformation: Laboratory Studies. Geophysical Monographs
897 36, 161-199.
898
899 Vannucchi, P., Bettelli, G., 2002. Mechanism of subduction accretion as implied from the broken
900 formations in the Apennines, Italy. Geology 30, 835–838.
901
902 Vernooij, M.G.C., den Brok, B., Kunze, K., 2006. Development of crystallographic preferred
903 orientations by nucleation and growth of new grains in experimentally deformed quartz single
904 crystals. Tectonophysics 427, 35-53.
905
906 Vogt, K., Gerya, T.V., Castro, A., 2012. Crustal growth at active continental margins: numerical
907 modeling. Physics of the Earth and Planetary Interiors 192–193, 1–20.
908
909 Vrolijk, P., Myers, G., Moore, J.C., 1988. Warm fluid migration along tectonic mélanges in the
910 Kodiak accretionary complex, Alaska. Journal of Geophysical Research: Solid Earth (1978–
911 2012), 93 (B9), 10313-10324.

912
913 Westbrook, G.K., Smith, M.J., 1983. Long decollements and mud volcanoes: Evidence from the
914 Barbados Ridge Complex for the role of high pore-fluid pressure in the development of an
915 accretionary complex. Geology 11, 279–283.
916
917 Williams, G.D., Powell C.M., Cooper M.A., 1989. Geometry and kinematics of inversion tectonics.
918 Geological Society, London, Special Publications 44 (1), 3-15.
919
920 Williams, H., Hatcher Jr., R.D., 1983. Appalachian suspect terranes. In: Hatcher, R.D., Jr.,
921 Williams, H., and Zietz, I. (Eds.), Contributions to the tectonics and geophysics of mountain chains:
922 Geological Society of America Special Memoir 158, 33–54.
923
924 Willner, A.P., 2005. Pressure–Temperature Evolution of a Late Palaeozoic paired Metamorphic
925 Belt in North-Central Chile (34 −35 30'S). Journal of Petrology 46, 1805–1833.
926
927 Willner, A.P., Thomson, S.N., Kröner, A., Wartho, J.A., Wijbrans, J.R., and Hervé, F., 2005. Time
928 markers for the evolution and exhumation history of a late Palaeozoic paired metamorphic belt in
929 north-central Chile (34 −35 30'S). Journal of Petrology 46, 1835–1858.
930
931 Yamamoto, Y., Nidaira, M., Ohta, Y., Ogawa, Y., 2009. Formation of chaotic rock units during
932 primary accretion processes: examples from the Miura-Boso accretionary complex, central Japan.
933 Island Arc 18, 496–512.
934
935 Yamamoto, Y., Ogawa, Y., Uchino, T., Muraoka, S., Chiba, T., 2007. Large-scale chaotically
936 mixed sedimentary body within the Late Pliocene to Pleistocene Chikura Group, Central Japan.
937 Island Arc 16, 505–507.
938
939 Yamamoto, Y., Ohta, Y., Ogawa, Y., 2000. Implication for the two-stage layer-parallel faults in the
940 context of the Izu forearc collision zone: Examples from the Miura accretionary prism, Central
941 Japan. Tectonophysics 325 (1–2), 133–144.
942
943
944 **Figure captions**
945

Figure 1. (a) Plate configuration of the west margin of South America (modified from Charrier et al., 2007). (b) Inset showing the main Chañaral mélange outcrops in northern Chile (modified from Bell, 1987). Mélange rocks, included in the Las Tórtolas Formation, are separated to highlight their contacts. Godoy and Welkner (2003) propose a different contact relations in the area of Carrizal Bajo, where mélange facies completely surround the rest of the Las Tórtolas Formation. **(**c) Detailed geological map of the study area at the S of Chañaral city. The locations of the structural analysis stations are indicated. Some of the metabasite outcrops indicated in the detailed map are taken from Godoy and Lara (1998). (d) Schematic cross section showing the structure of the study area, including both structural domains described below. Location in Fig. 1c.

Figure 2. Field photographs of some outstanding lithological and structural features of the study area. Chañaral mélange and the rest of the Las Tórtolas Formation are in contact through the Infieles fault (a, b). The fault contact show dextral reverse kinematics (a) and 2-5 m in thickness (b). Thrust-propagation folds (c) are one of the most outstandings structural characteristics of the Las Tórtolas Formation to the east of the Infieles fault, whereas some quartzite layers show folded pinch and swell structures (d). Chañaral mélange is mainly comprised of quartzite blocks in a phyllitic matrix (e), with minor amounts of intensely deformed conglomerates (f), shales (g) and chloritized basic rocks (h).

Figure 3. Microphotographs showing characteristic fabrics of the studied samples. Most are cross-polarized light images except (c), which is a plane-polarized light image. In (h) a gypsum plate is incorporated. (a) and (c) are from more impure areas whereas the rest correspond to purer quartzite areas. (a) Rounded, elliptical, sub-rectangular and irregular grains with little internal deformation evidenced by incipient undulose to sweeping extinction. Sub-rectangular and elliptical grains are subparallel with the rough foliation defined by micas. Mica enrichment is apparent at long straight quartz grain boundaries. (b) Quartz vein. Irregularly shaped quartz grains showing undulose, patchy and sweeping extinction. (c) Iron hydroxide and mica enrichment along long straight boundaries of sub-rectangular quartz grains. (d) Coarse quartz grains with serrated high-angle and subgrain boundaries, recrystallization bulges (bottom-left) and isolated grains (center). (e) Core-and-mantle structure. The coarse quartz grain shows newly recrystallized grains associated with a fracture. (f) Core-and-mantle structure. The coarse quartz grain presents a fracture along which newly recrystallized grain are located. (g) and (h) Old, irregular, highly strained quartz grains (delimitated in (g) and recognized in (h) as the large orange grain in the center) appear partially replaced by strain-free, fine grained recrystallized quartz grains. 120º angle triple junctions are defined by grain and subgrain boundaries.

Figure 4. Field photographs of the main characteristics of the mélange facies. (a) Quartzite blocks showing a prolate mesoscopic shape. Phyllite matrix in these areas (inset) (L domains) are characterized by "pencil structure". (b) Tight to isoclinal folds. The prominent quartzite object points the fold axis. (c) Spaced crenulation foliation related to small scale kink folds in the phyllitic mélange matrix. (d) Asymmetric objects (basic rocks) are used to determine the shear zone kinematics. (e) S-C structures are observed as one of the main structures actives during the mélange formation. (f) Boudinage and pinch and swell structures are mainly observed affecting to the quartzite layers, albeit some syn- post-deformational dykes show boudinage structures.

Figure 5. Structural map of the study area showing the deformation partitioning between the mélange facies (ductile zone) and the Las Tórtolas Formation (brittle-ductile zone). According to field observations in the study area, mélange zones dominated by linear and linear-planar fabric are named as L and L-S domains. Equal-area, lower hemisphere spherical projections of linear and planar fabrics measured in the study área are presented. Statistical axial planes have been calculated for comparison with measured major folds.

Figure 6. Figure showing the sampling process to obtain the SPO results in Qtz microfabric. Three orthogonal sections are obtained from the oriented quartzite objects (a). High resolution microphotographs (b) taken from oriented surfaces (a, b, c) are analyzed with the SPO 2003 software (c) (Launeau and Robin, 2005). The orientation and shape of the 3D fabric ellipsoid (d) was obtained using Ellipsoid 2003 software (Launeau and Robin, 2005). See text for further details.

Figure 7. (a) Results of the Qtz microfabric SPO measurement at the 18 selected stations. Shape (Flinn, 1962), intensity (Nadai, 1950) and shape (Lode, 1926) parameters are indicated in each site (Table 2). (b) Flinn (1962) diagram showing the mesoscopic quartzite blocks measurements (Table 1) in comparison with microfabric SPO results.

Figure 8. Tentative geodynamic evolution model of the western active margin of South America. Crustal scale cross sections of the convergent margin are modified from Mpodozis and Ramos (1989) (a), Mpodozis and Kay (1992) (c), and Mpodozis and Ramos (2008) (e). Depths and isothermal profiles are traced according to the 2D coupled petrological–thermomechanical numerical model for compressional arcs in subduction zones (Vogt et al., 2012). Granitic melts generation in the mantle lithosphere is based on hybrid plumes and relamination processes (Castro et al., 2010, 2013). Accordingly, in (a), (c) and (e), the red areas represent both the cold, mantle wedge plumes (Vogt et al., 2012; Castro et al., 2010, 2013) composed by a mixture of sediments, continental and oceanic rocks, as well as the silicic magmas resulting form their partial melting. The purple body in (e) symbolizes basic magmas generated from direct melting of the ultrabasic envelope around hybrid plumes. The yellow areas in (c) represent the anatectic melts (S-type

granitoids) generated during Late Permian to Triassic. (b) and (d) are schematic not to scale blocks that show the structural organization and the location of Chañaral mélange and the Las Tórtolas Formation during the evolution of the accretionary complex between Late Paleozoic to Early Jurassic. The location of the mélange facies is based on the temperatures obtained in this work by describing the intracrystalline deformation mechanisms, combined with the isothermal profile. Similar depths of ca. 30 Km have been estimated in the metamorphic mineral assemblages of the subduction-related rocks in Pichilemu region (Hyppolito et al., 2014b).

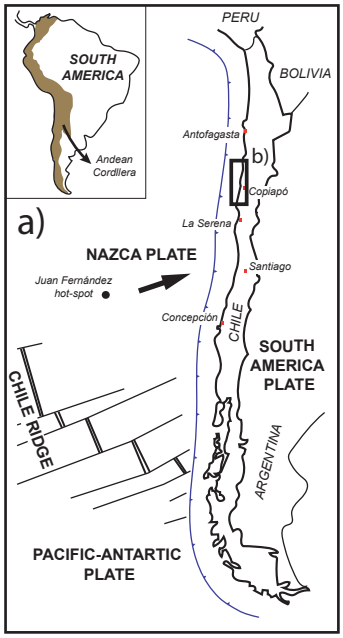

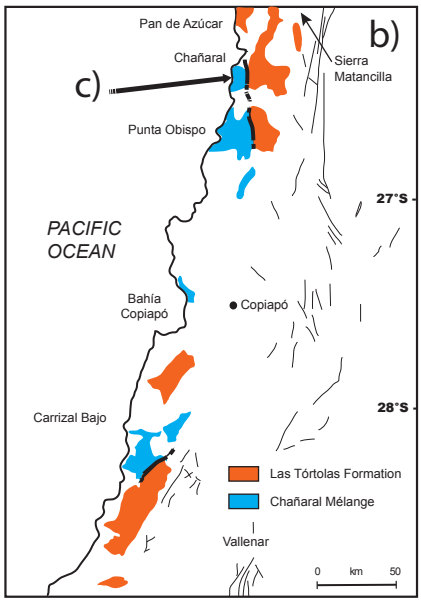

LEGEND

- Las Tórtolas Formation (Chañaral epimetamorphic complex)
- Chañaral melange *Hornfelses
- Andesitic rocks
- Quartzite blocks
- Limestones
- Conglomerates
- Metabasites

Intrusive dykes

- Tonalites
- Gabbros

- Infieles fault contact
- Thrust fault
- Transcurrent fault
- Primary foliation (S0)
- Tectonic foliation (S1)
- Fold axis
- Lineation
- Structural analysis station

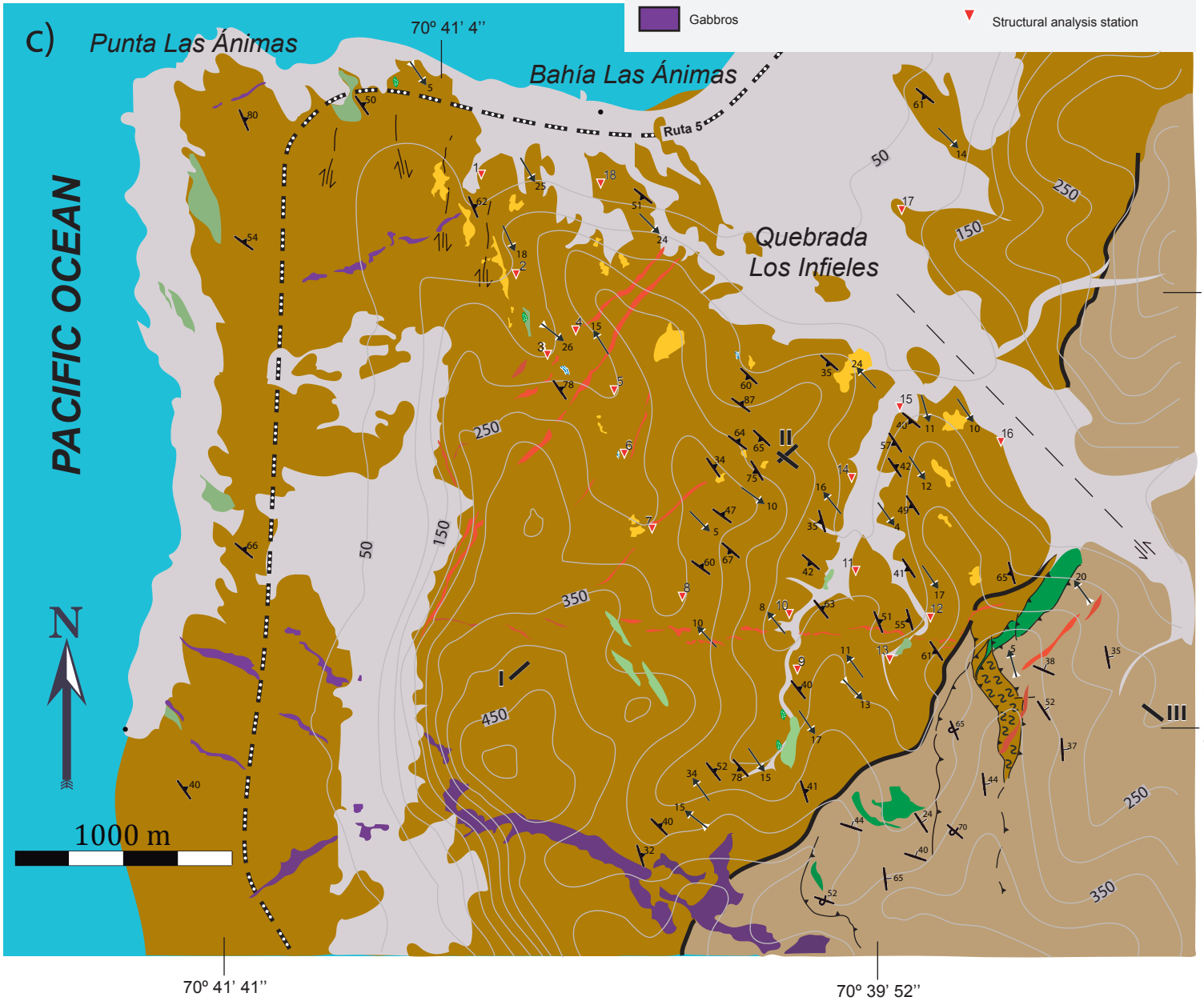

d)

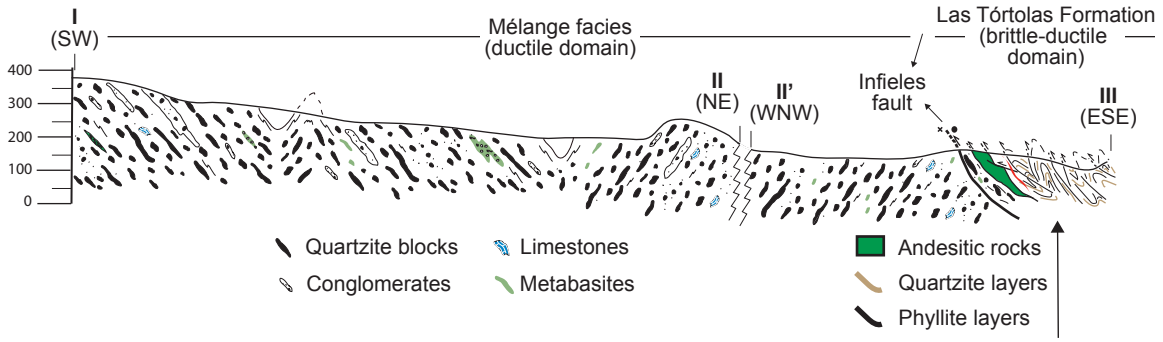
I
(SW)
Mélange facies
(ductile domain)
Las Tórtolas Formation
(brittle-ductile
domain)
II
(NE)
II'
(WNW)
Infieles
fault
III
(ESE)
400
300
200
100
0
Quartzite blocks
Conglomerates
Limestones
Metabasites
Andesitic rocks
Quartzite layers
Phyllite layers

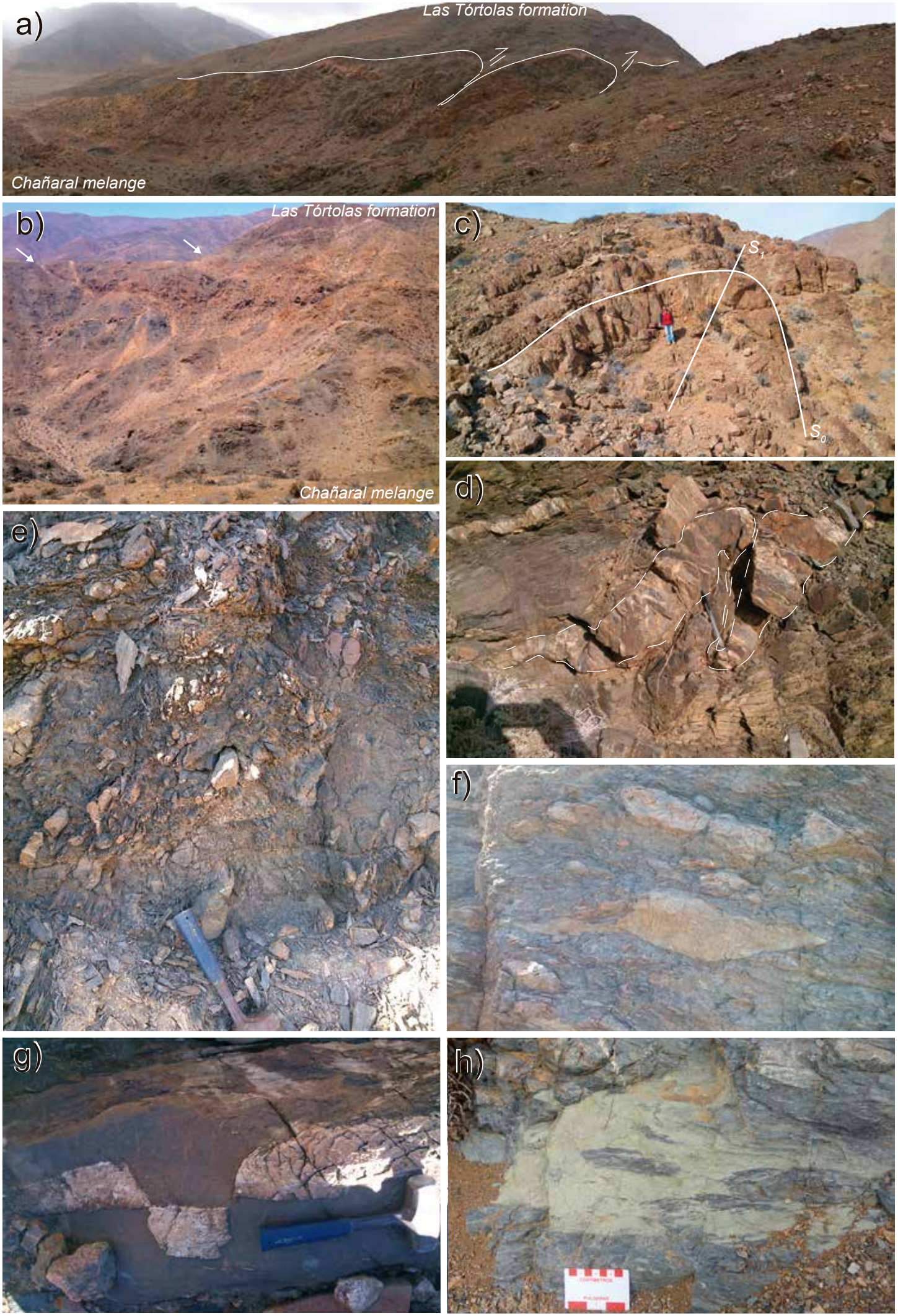
a)
Las Tórtolas formation
Chañaral melange
b)
Las Tórtolas formation
Chañaral melange
c)
S_1
S_0
d)
e)
f)
g)
h)

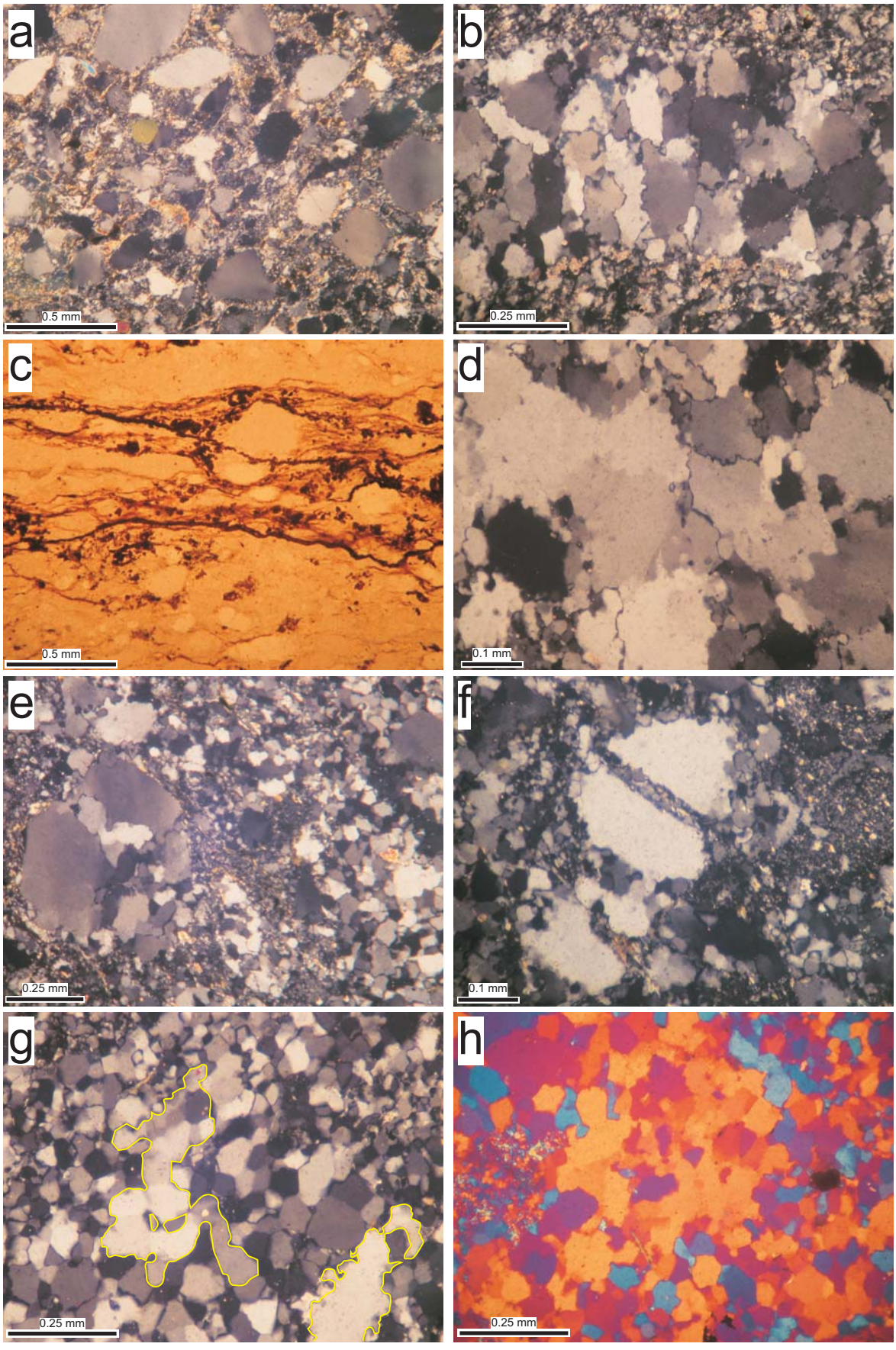

Fuentes et al. - Figure 3

Figure 3.- Microphotographs showing characteristic fabrics of the studied samples. Most are cross-polarized light images except (c), which is a plane-polarized light image. In (h) a gypsum plate is incorporated. (a) and (c) are from more impure areas whereas the rest correspond to purer quartzite areas. (a) Rounded, elliptical, sub-rectangular and irregular grains with little internal deformation evidenced by incipient undulose to sweeping extinction. Sub-rectangular and elliptical grains are subparallel with the rough foliation defined by micas. Mica enrichment is apparent at long straight quartz grain boundaries. (b) Quartz vein. Irregularly shaped quartz grains showing undulose, patchy and sweeping extinction. (c) Iron hydroxide and mica enrichment along long straight boundaries of sub-rectangular quartz grains. (d) Coarse quartz grains with serrated high-angle and subgrain boundaries, recrystallization bulges (bottom-left) and isolated grains (center). (e) Core-and-mantle structure. The coarse quartz grain shows newly recrystallized grains associated with a fracture. (f) Core-and-mantle structure. The coarse quartz grain presents a fracture along which newly recrystallized grain are located. (g) and (h) Old, irregular, highly strained quartz grains (delimitated in g and recognized in h as the large orange grain in the center) appear partially replaced by strain-free, fine grained recrystallized quartz grains. 120º angle triple junctions are defined by grain and subgrain boundaries.


a)
b)
c)
d)
CENTIMETROS
PULGADAS
e)
S
C
f)

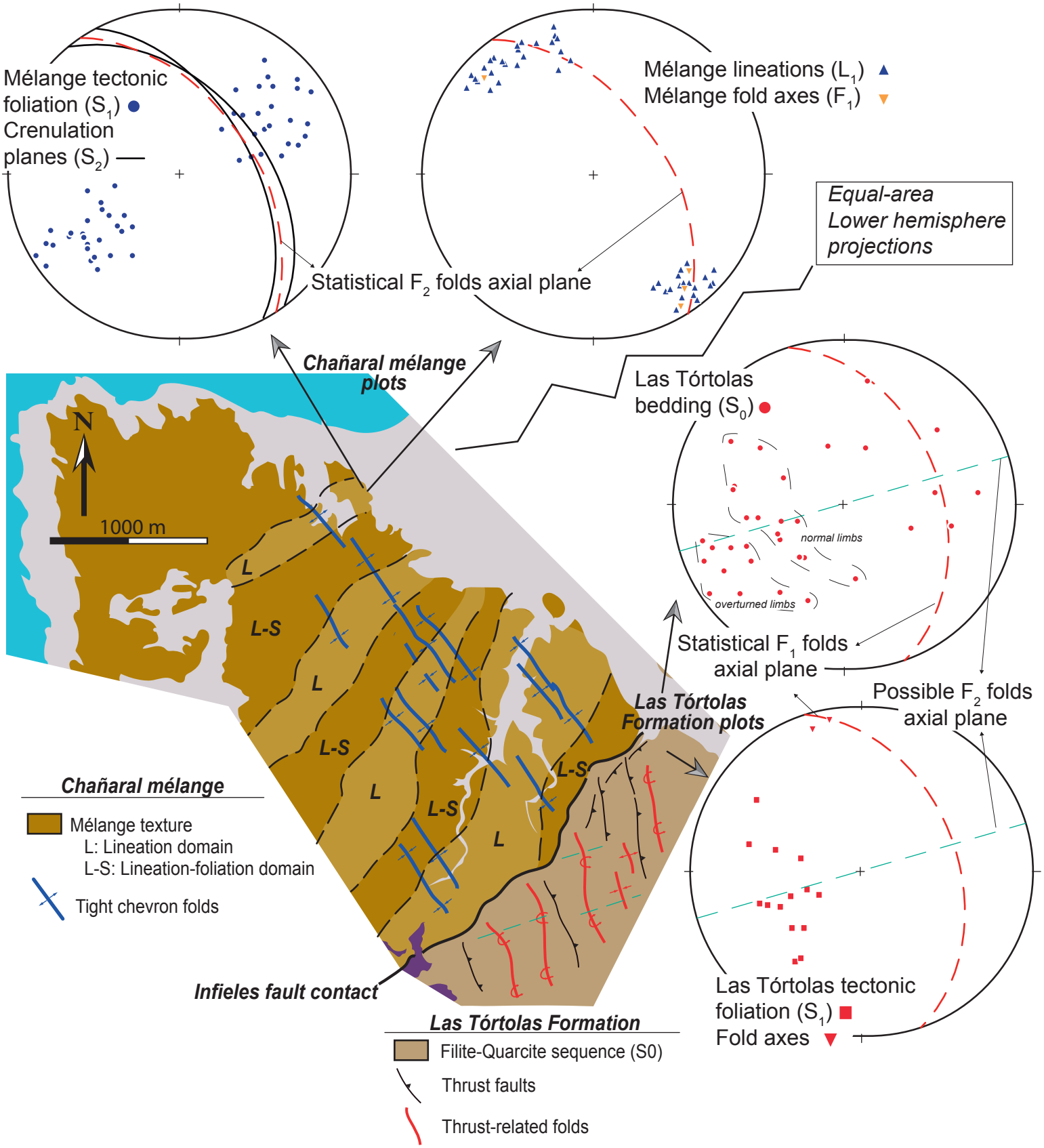
Mélange tectonic foliation (S_1)
Crenulation planes (S_2)
Statistical F_2 folds axial plane
Mélange lineations (L_1)
Mélange fold axes (F_1)
Equal-area
Lower hemisphere
projections
Chañaral mélange plots
Las Tórtolas bedding (S_0)
normal limbs
overturned limbs
Statistical F_1 folds axial plane
Possible F_2 folds axial plane
Las Tórtolas Formation plots
N
1000 m
L
L-S
Chañaral mélange
Mélange texture
L: Lineation domain
L-S: Lineation-foliation domain
Tight chevron folds
Infieles fault contact
Las Tórtolas tectonic foliation (S_1)
Fold axes
Las Tórtolas Formation
Filite-Quarcite sequence (S0)
Thrust faults
Thrust-related folds

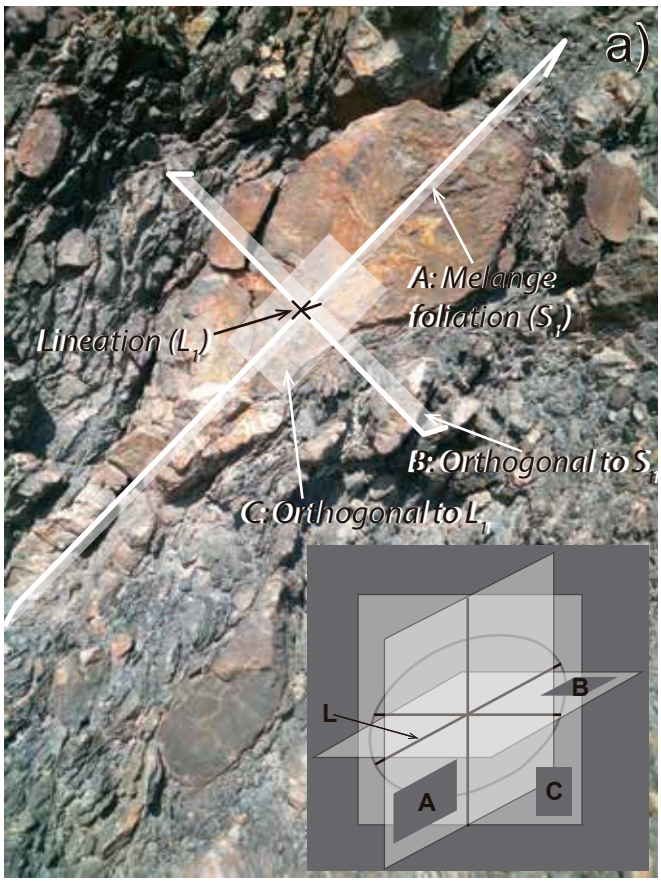
a)
A: Melange foliation (S_1)
Lineation (L_1)
B: Orthogonal to S_1
C: Orthogonal to L_1
L
B
A
C

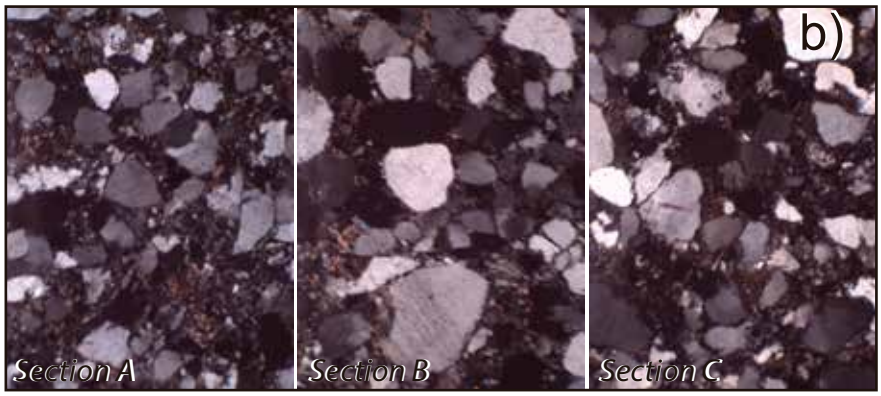
b)
Section A
Section B
Section C

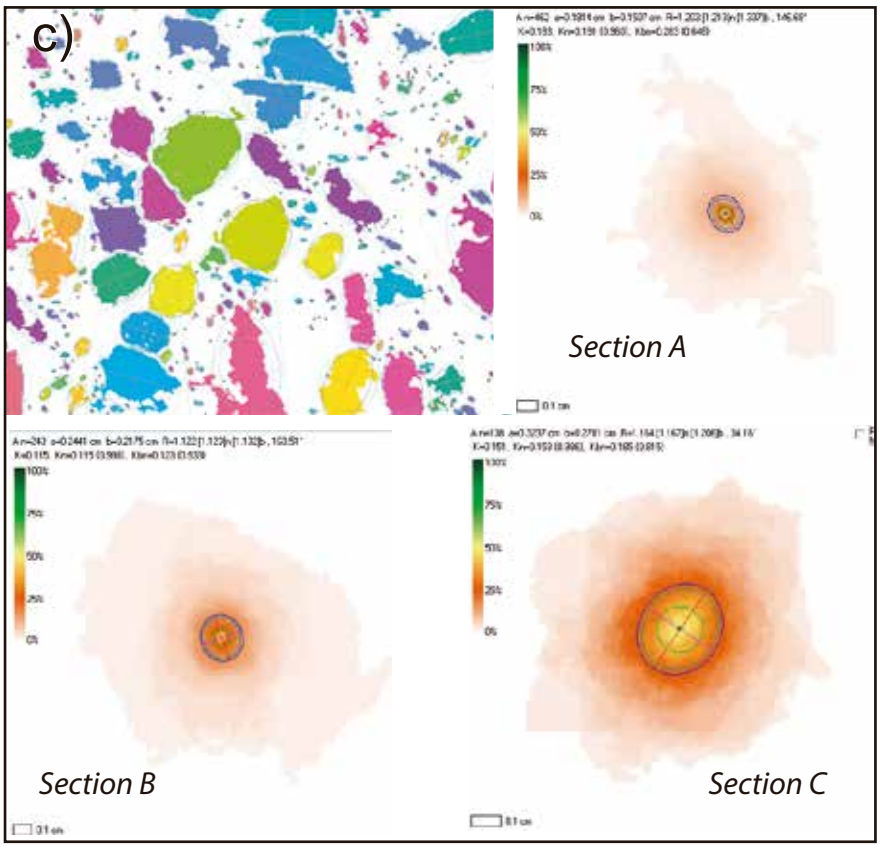
c)
Section A
Section B
Section C

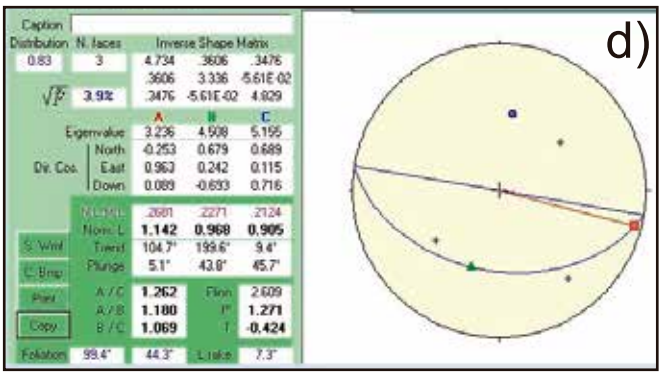
Caption
Distribution
N. faces
Inverse Shape Matrix
0.83
3
4.734
.3606
.3476
.3606
3.336
-5.61E-02
.3476
-5.61E-02
4.929
3.9%
A
B
C
Eigenvalue
3.236
4.508
5.195
Dir. Cos.
North
-0.253
0.679
0.689
East
0.963
0.242
0.115
Down
0.089
-0.693
0.716
.2681
.2271
.2124
Norm. L
1.142
0.968
0.905
Trend
104.7°
199.6°
9.4°
Plunge
5.1°
43.8°
45.7°
S. Wnt
C. Bmp
Print
Copy
A / C
1.262
Flinn
2.609
A / B
1.180
F
1.271
B / C
1.069
T
-0.424
Foliation
99.4°
44.3°
Lineation
7.3°
d)

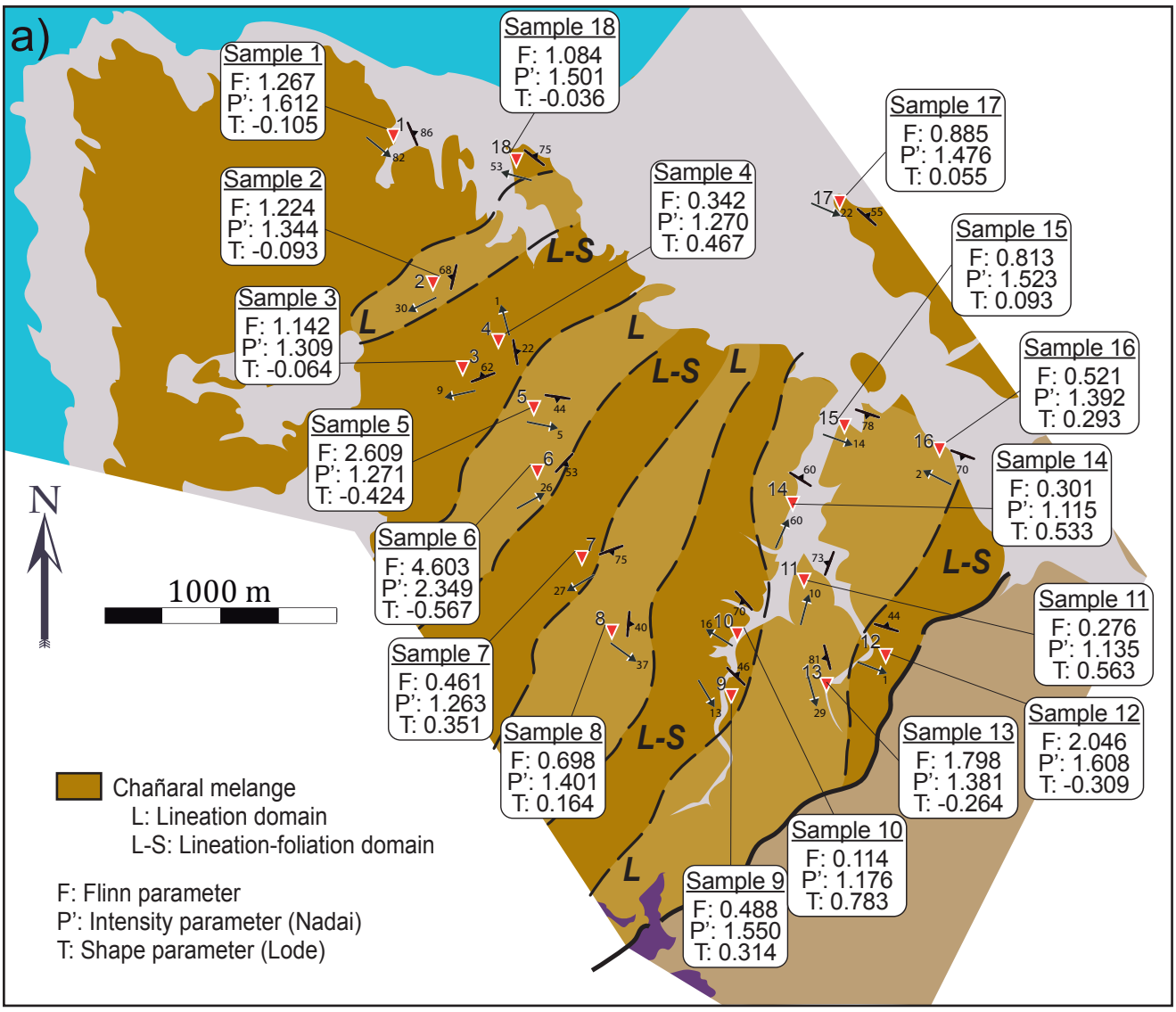
a)
Sample 1
F: 1.267
P': 1.612
T: -0.105
Sample 2
F: 1.224
P': 1.344
T: -0.093
Sample 3
F: 1.142
P': 1.309
T: -0.064
Sample 4
F: 0.342
P': 1.270
T: 0.467
Sample 5
F: 2.609
P': 1.271
T: -0.424
Sample 6
F: 4.603
P': 2.349
T: -0.567
Sample 7
F: 0.461
P': 1.263
T: 0.351
Sample 8
F: 0.698
P': 1.401
T: 0.164
Sample 9
F: 0.488
P': 1.550
T: 0.314
Sample 10
F: 0.114
P': 1.176
T: 0.783
Sample 11
F: 0.276
P': 1.135
T: 0.563
Sample 12
F: 2.046
P': 1.608
T: -0.309
Sample 13
F: 1.798
P': 1.381
T: -0.264
Sample 14
F: 0.301
P': 1.115
T: 0.533
Sample 15
F: 0.813
P': 1.523
T: 0.093
Sample 16
F: 0.521
P': 1.392
T: 0.293
Sample 17
F: 0.885
P': 1.476
T: 0.055
Sample 18
F: 1.084
P': 1.501
T: -0.036
L
L-S
N
1000 m
Chañaral melange
L: Lineation domain
L-S: Lineation-foliation domain
F: Flinn parameter
P': Intensity parameter (Nadai)
T: Shape parameter (Lode)

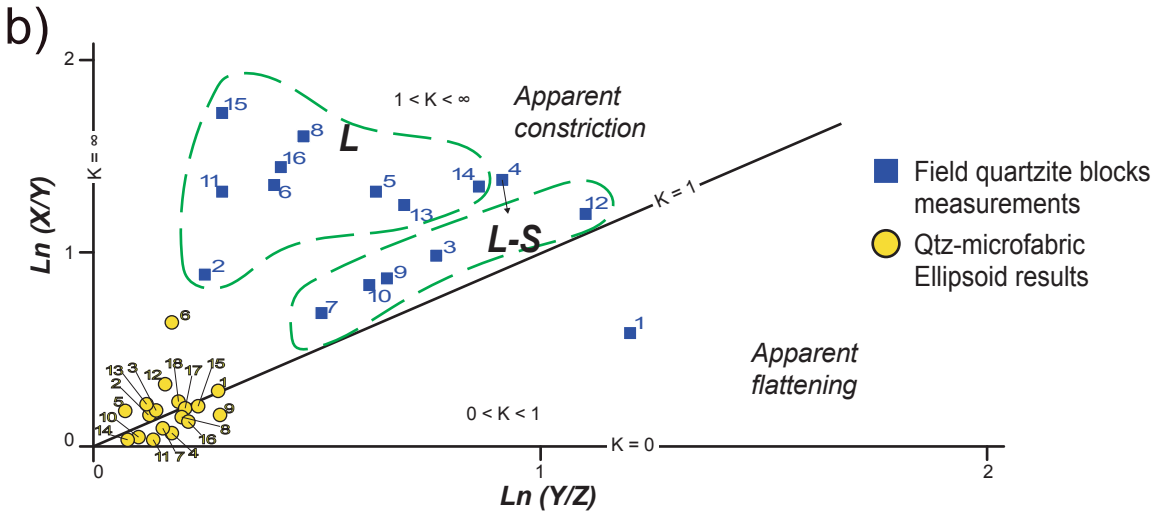
b)
Ln (X/Y)
Ln (Y/Z)
K = ∞
K = 1
K = 0
1 < K < ∞
0 < K < 1
Apparent constriction
Apparent flattening
L
L-S
Field quartzite blocks measurements
Qtz-microfabric Ellipsoid results

a) Late Paleozoic
(fast convergence)

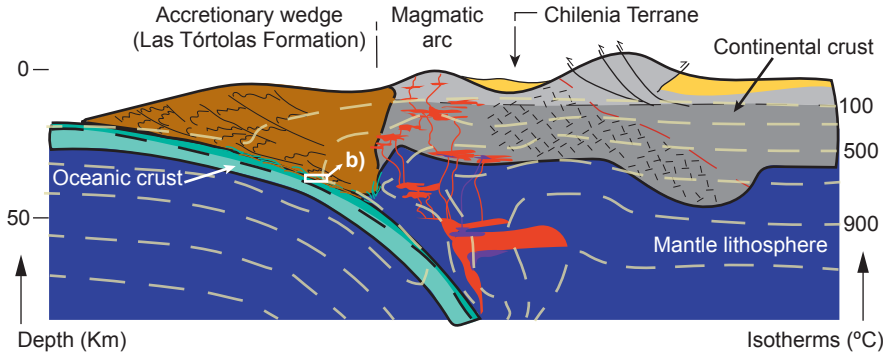

b)

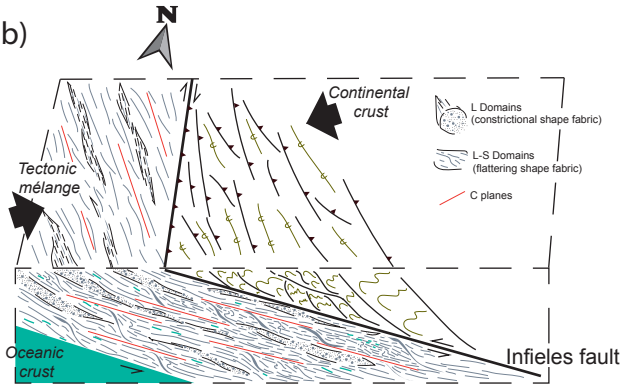

c) Late Permian to Triassic
(slow convergence or subduction cessation)

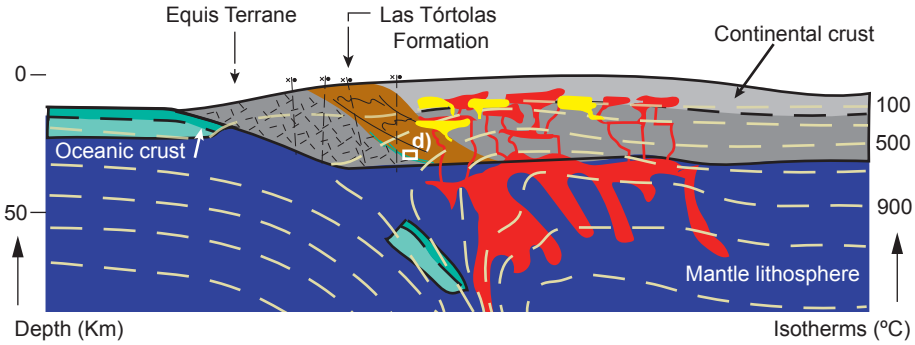

d)

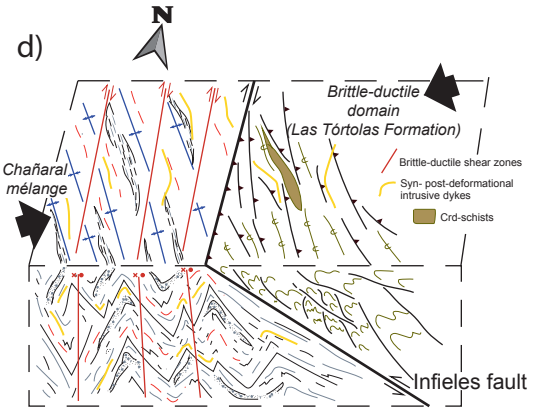

e) Early Jurassic
(subduction reactivation)

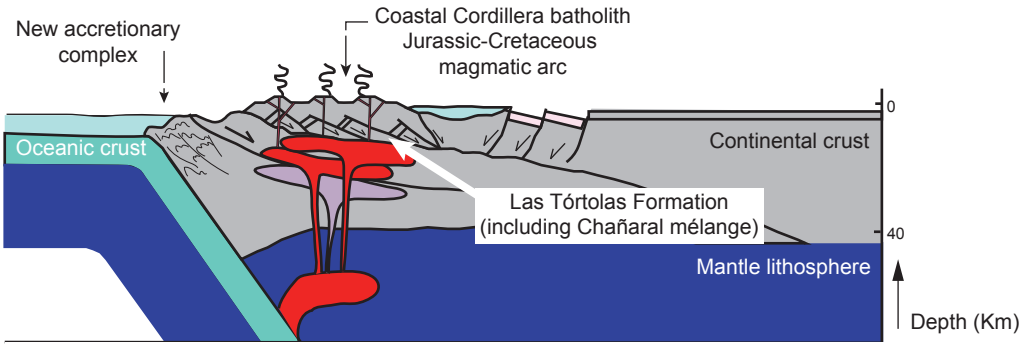

Table 1

Data of the mesoscopic SPO measured at the 18 stations of the study area

Station	Measured	Ellipsoid axis (cm)			Aspect ratios			Ellipsoid parameters
	foliation	A	B	C	A/C	A/B	B/C	Flinn Shape
1	N42W/58NE	45	25	7,5	6,0	1,8	3,3	0,5
2	N24W/90	44	18	14	3,1	2,4	1,3	3,6
3	N27W/44NE	150	56	26	5,8	2,7	2,2	1,3
4	N2W/52NE	60	15	6	10,0	4,0	2,5	1,5
5	N38W/46NE	60	16	8,5	7,1	3,8	1,9	2,1
6	N24W/30NE	70	18	12	5,8	3,9	1,5	3,3
7	N20W/58NE	150	75	45	3,3	2,0	1,7	1,4
8	N32W/70NE	60	12	7,5	8,0	5,0	1,6	3,4
9	N30W/70NE	60	25	13	4,6	2,4	1,9	1,3
10	N30W/62NE	60	26	14	4,3	2,3	1,9	1,4
11	N40W/70NE	45	12	9	5,0	3,8	1,3	4,6
12	N36W/70NE	100	30	10	10,0	3,3	3,0	1,1
13	N40W/55NE	70	20	10	7,0	3,5	2,0	1,8
14	N35W/70NE	50	13	5,5	9,1	3,8	2,4	1,6
15	N35W/70NE	90	16	12	7,5	5,6	1,3	6,0
16	N38W/70NE	80	19	12,5	6,4	4,2	1,5	3,4
17	N50W/60NE	-	-	-	-	-	-	-
18	N40W/90	-	-	-	-	-	-	-

Table 2

Data of the Qtz microfabric SPO calculated at the 18 sampled stations in the Chañaral mélange using Ellipsoid 2003 (Robin, 2002; Launeau and Robin, 2005).

Station	Calculated	Ellipsoid axis			Normalized axis values			Aspect ratios			Ellipsoid parameters			Normallized
	foliation	A	B	C	A	B	C	A/C	A/B	B/C	Flinn	P' (Nadai)	T (Lode)	deviation (%)
1	N24W/86NE	81.8°→ 130.2°	7.4° →336.1°	3.6° →245.6°	1.278	0.984	0.796	1.607	1.299	1.326	1.267	1.612	-0.105	12.6
2	N16E/68NW	30°→ 209°	51.4°→ 345.1°	22°→ 105.5°	1.164	0.991	0.867	1.343	1.175	1.143	1.224	1.344	-0.093	2.6
3	N72E/62NW	8.7°→ 256.2°	60.4°→ 1.9°	28°→ 161.5°	1.147	0.994	0.877	1.308	1.153	1.134	1.142	1.309	-0.064	3.5
4	N6W/22NE	0.3°→ 354.7°	22°→ 84.8°	68°→ 264°	1.102	1.037	0.875	1.259	1.063	1.184	0.342	1.27	0.467	6.5
5	N81W/44SW	5.1°→ 104.7°	43.8°→ 199.6°	45.7°→ 9.4°	1.142	0.968	0.905	1.262	1.18	1.069	2.609	1.271	-0.424	3.9
6	N38E/53SE	26.1°→ 59.8°	41.4°→ 175.3°	37.5°→ 307.8°	1.608	0.86	0.723	2.223	1.87	1.189	4.603	2.349	-0.567	22.3
7	N73E/75SE	27.4°→ 244.8°	58.3°→ 97.6°	14.6°→ 342.6	1.106	1.027	0.88	1.257	1.077	1.167	0.461	1.263	0.351	2
8	N5E/40SE	36.5°→ 122°	13.8°→ 21.6°	50.1°→ 274.5°	1.171	1.018	0.838	1.398	1.15	1.215	0.698	1.401	0.164	16.3
9	N40W/46NE	13.2°→ 152.8°	43.1°→ 255.5°	43.9°→ 49.8°	1.212	1.046	0.789	1.537	1.159	1.326	0.488	1.55	0.314	8.1
10	N69W/70SW	15.9°→ 297.4°	64.5°→ 64.1°	19.4°→ 201.7°	1.05	1.023	0.931	1.128	1.027	1.098	0.276	1.135	0.563	8.6
11	N22E/73NW	9.8°→ 19.4°	70.3°→ 260.7°	16.9°→ 112.4°	1.056	1.039	0.911	1.159	1.016	1.14	0.114	1.176	0.783	1.8
12	N73W/44NE	0.7°→ 106.7°	44.2°→ 16°	45.8°→ 197.4°	1.292	0.953	0.812	1.592	1.356	1.174	2.046	1.608	-0.309	14.1
13	N18W/81SW	29.3°→ 166.9	59.3°→ 328.2°	8.2°→ 72.3°	1.189	0.972	0.865	1.375	1.223	1.124	1.798	1.381	-0.264	4.1
14	N53W/60NE	60.2°→ 30.5°	2.7°→ 125.2°	29.7°→ 216.7	1.044	1.019	0.94	1.11	1.025	1.083	0.301	1.115	0.533	6.5
15	N70W/78SW	13.9°→ 113.1	71.1°→ 249.4°	12.5°→ 20°	1.225	1.013	0.806	1.52	1.209	1.257	0.813	1.523	0.093	3.3
16	N65W/70SW	1.9°→ 295.8°	70.3°→ 200.5°	19.6°→ 26.4°	1.158	1.032	0.837	1.384	1.122	1.234	0.521	1.392	0.293	17.8
17	N50W/55NE	22.3°→ 113.2°	46.6°→ 357.5°	34.9°→ 219.8°	1.21	1.007	0.821	1.474	1.201	1.227	0.885	1.476	0.055	5
18	N53W/75NE	52.6°→ 286.9°	33.4°→ 137.4°	14.9°→ 37.3°	1.227	0.995	0.819	1.499	1.233	1.215	1.084	1.501	-0.036	10.5